JOURNAL OF GEOPHYSICAL RESEARCH, VOL. 95, NO. C5, PAGES 7185–7200, MAY 15, 1990

Low-Frequency, Motionally Induced Electromagnetic Fields in the Ocean 1. Theory

ALAN D. CHAVE

AT&T Bell Laboratories, Murray Hill, New Jersey

DOUGLAS S. LUTHER

Scripps Institution of Oceanography, La Jolla, California

The theory of electromagnetic induction by motional sources in the ocean is examined from a first principles point of view. The electromagnetic field is expanded mathematically in poloidal and toroidal magnetic modes based on the Helmholtz decomposition. After deriving a set of Green functions for the modes in an unbounded ocean of constant depth and conductivity underlain by an arbitrary one-dimensional conducting earth, a set of exact integral equations are obtained which describe the induction process in an ocean of vertically varying conductivity. Approximate solutions are constructed for the low-frequency (subinertial) limit where the horizontal length scale of the flow is large compared to the water depth, the effect of self induction is weak, and the vertical velocity is negligible, explicitly yielding complex relationships between the vertically-integrated, conductivity-weighted horizontal water velocity and the horizontal electric and three component magnetic fields and accounting for interactions with the conductive earth. After introducing geophysically reasonable models for the conductivity structures of the ocean and earth, these reduce to a spatially smoothed proportionality between the electromagnetic field components and the vertically-integrated, conductivity-weighted horizontal water velocity. An upper bound of a few times the water depth for the lateral averaging scale of the horizontal electric field is derived, and its constant of proportionality is shown to be nearly 1 for most of the deep ocean based on geophysical arguments. The magnetic field is shown to have a similar form but is a relatively weak, larger-scale average of the velocity field. Because vertical variations in the conductivity of seawater largely reflect its thermal structure and are weak beneath the thermocline, the horizontal electric field is a spatially filtered version of the true water velocity which strongly attenuates the influence of baroclinicity and accentuates the barotropic component. This is quantified using conductivity profiles and velocity information from a variety of locations.

INTRODUCTION

Natural electromagnetic fields in the oceans are induced by both external, ionospheric and magnetospheric, electric current systems and by the dynamo interaction of ocean water currents with the earth's magnetic field. The former have been fairly well characterized at the surface of the earth and are often measured during geophysical investigations of its electrical structure. While the existence of motional electric currents in the ocean was first postulated by *Faraday* [1832], oceanic electromagnetic fields remain less well understood, primarily due to the difficulty of collecting in situ observations.

Theoretical studies of motional induction divide naturally at the inertial frequency due to changes in their physical behavior. Only the subinertial case will be considered in this paper, and the ocean tides are specifically excluded from treatment. of long-period motional electromagnetic fields post-date World War II and began with the theoretical work of *Stommel* [1948], *Longuet-Higgins* [1949], *Malkus and Stern* [1952], and *Longuet-Higgins et al.* [1954]. These investigations led to some early measurements on submarine cables [e.g., *Wertheim*, 1954] and the development of the geomagnetic electrokinetograph (GEK) [*von Arx*, 1950]. The most complete theoretical investigation of low-frequency motional induction available is due to *Sanford* [1971]. This work has formed the basis for the successful interpretation of submarine cable measurements in terms of transport [*Sanford*, 1982; *Larsen and Sanford*, 1985] and spawned some novel oceanographic instrumentation [*Sanford et al.*, 1985]. Despite the obvious utility of the theoretical studies, the results are formally deficient in two respects. First, while it has long been recognized that motional horizontal electric and magnetic fields are proportional to the vertically-integrated, conductivity-weighted horizontal water velocity, most of the investigations fail to demonstrate this explicitly. Furthermore, the importance of conductivity weighting in oceanographic applications has received relatively little emphasis. Second, while it is known that electromagnetic interactions with the conductive material beneath the seafloor may be significant, due to analytical complexity it is common to model the earth in a simple and probably unrealistic manner. Because of these limitations and increasing oceanographic experimental activity using electromagnetic tools [e.g., *Sanford*, 1986; *Luther et al.*, 1987], it is appropriate to re-examine the motional induction problem in its entirety.

In this paper, the relationships between all six components of the electromagnetic field and the water velocity are derived from first principles in the low-frequency limit where the horizontal length scale of the flow is greater than the water depth and the effect of self-induction is weak. The electromagnetic fields with a motional source are decomposed into poloidal and toroidal magnetic modes using a formalism suggested by *Backus* [1986]. This approach allows an arbitrary one-dimensional electrical structure for the earth beneath the sea to be modeled in a straightforward manner. Using a set of Green functions valid for an unbounded ocean of constant conduc-

Paper number 90JC00189.
0148-0227/90/90JC-00189$05.00

tivity and depth, an exact set of integral equations are derived for the primary and secondary electromagnetic fields in an ocean of vertically varying conductivity. Approximate solutions for the integral equations can be constructed that explicitly yield the expected relationship with the vertically-integrated, conductivity-weighted horizontal water velocity in the low-frequency limit. The effect of the earth's electrical structure on the electromagnetic fields is then examined in detail. While a complex relationship between the frequency-wave number dependence of the water velocity field and the earth's electrical structure is formally required, it is shown that a geophysically reasonable model for the structure under the deep ocean floor leads only to weak coupling, and a simple proportionality between the horizontal electric field and the vertically-integrated, conductivity-weighted horizontal water velocity smoothed over a horizontal scale of no more than a few times the water depth obtains. The constant of proportionality is approximately 1, reflecting the minimal extent of current leakage into the geophysical deep seafloor. For the magnetic field, the conclusions are similar, although the horizontal averaging distance is larger and the fields are very weak. Because the depth dependence of seawater conductivity largely reflects its thermal structure and is nearly constant beneath the main thermocline, the vertical integration property of the electromagnetic field dramatically reduces the influence of the baroclinic (depth-dependent) field, yielding a filtered version of the velocity that is usually dominated by the barotropic (depth-averaged) component.

The next four sections of the paper and the four appendices contain the complete mathematical development of the theory of low-frequency motional induction. Readers interested in the key results and oceanographic applications may wish to skim these sections and concentrate on the last four parts of the paper. As an aid to the reader, the symbols are summarized in the notation section at the end of the paper together with the number of the equation where each quantity is defined. Vector quantities are always indicated by boldface type.

In a separate paper (D.S. Luther et al., Low-frequency, motionally-induced electromagnetic fields in the ocean, 2, electric field and Eulerian current comparison from BEMPEX, submitted to *Journal of Geophysical Research*, 1990; hereinafter designated Luther et al., 1990) the theory is verified observationally by comparing the water velocity as measured directly by a mechanical current meter mooring with contemporaneous records of the seafloor electric and magnetic fields.

GOVERNING EQUATIONS

For the length and time scales of interest in motional induction in the subinertial range, the quasi-static or pre-Maxwell approximation to the full Maxwell equations is sufficient. This limit involves neglect of displacement current, polarization current, and advected charge in comparison to the conduction current. For a moving medium and with the magnetic permeability μ that of free space everywhere, the resulting equations are

$$\nabla\cdot\mathbf{B} = 0 \tag{1}$$

$$\nabla\times\mathbf{E} + \partial_t\mathbf{B} = 0 \tag{2}$$

$$\nabla\times\mathbf{B} - \mu\mathbf{J} = 0 \tag{3}$$

where the electric current density is given by

$$\mathbf{J} = \sigma(\mathbf{E} + \mathbf{v}\times\mathbf{B}) \tag{4}$$

Since the induced magnetic induction is very weak compared to the earth's main field, the Lorentz force on water particles is many orders of magnitude smaller than hydrodynamic ones. As a result, the total magnetic induction $\mathbf{B}$ in (4) may be approximated by that of the earth $\mathbf{F}$ that is assumed to be both sourceless and static. The electric current (4) is then the sum of an induced part $\mathbf{I} = \sigma\mathbf{E}$ and a source term $\sigma(\mathbf{v}\times\mathbf{F})$. Note that the electric field in (2)–(4) is the value for an observer fixed to the earth; for a reference frame moving at a relative velocity $\mathbf{v}_r$ and neglecting relativistic effects, the electric field is $\mathbf{E}' = \mathbf{E} + \mathbf{v}_r\times\mathbf{F}$, while the magnetic induction $\mathbf{B}$ is unchanged.

It is essential to understand the role which electric charge plays under the quasi-static approximation. Neglect of the displacement current in (3) requires that the electric current density $\mathbf{J}$ be divergence-free, and the time rate of change of the charge density is zero to the same level of approximation. In fact, the electric currents which distribute electric charges occur on a time scale of $O(\nu/\sigma)$ (where ν is the electrical permittivity) that is instantaneous compared to the time scale of interest, so that they do not produce any significant time-varying magnetic fields. However, the electric fields produced by charges which move into place with seemingly infinite speed are quite important and are not removed by the approximation. The quasi-static scaling is a singular perturbation problem with some interesting consequences at breakdown; see *Backus* [1982] for a discussion.

The pre-Maxwell equations will be solved in terms of poloidal and toroidal magnetic (PM and TM) modes based on the Helmholtz representation of a vector field. The modal form is useful because it reduces the physics into two relatively simple and independent parts. The PM mode is marked by electric currents flowing in horizontal planes that couple by induction, and has no vertical electric field component. The TM mode is associated with electric currents flowing in planes containing the vertical, and has no vertical magnetic field component. The TM mode magnetic field vanishes at the Earth's surface, and is not observable outside of it. Electric charges associated with conductivity gradients affect only the TM mode. This physical approach should be contrasted with one based either on the magnetic vector potential or directly on the fields in which interactions with conducting material are difficult to handle, necessitating simplifications that are often geophysically untenable.

Using the Helmholtz representation theorem defined in Appendix A and (1), the magnetic induction may be written

$$\mathbf{B} = \hat{z}\times\nabla_h\Pi + \nabla_h\partial_z\Psi - \nabla_h^2\Psi\hat{z} \tag{5}$$

where Π and Ψ are scalar functions which represent the TM and PM modes. Let the source current in (4) be expanded in a similar way so that

$$\sigma(\mathbf{v}\times\mathbf{F}) = \Xi\hat{z} + \nabla_h\mathrm{T} + \hat{z}\times\nabla_h\mathrm{Y} \tag{6}$$

Under the condition that the Earth's conductivity varies only vertically and that the magnetic permeability has the free space value everywhere, it is proved in Appendix A that the modal scalars satisfy the differential equations

$$\nabla^2\Psi - \mu\sigma\partial_t\Psi = \mu\mathrm{Y} \tag{7}$$

and

$$\nabla_h^2\Pi + \sigma\partial_z(\partial_z\Pi/\sigma) - \mu\sigma\partial_t\Pi = \mu\Xi - \mu\sigma\partial_z(\mathrm{T}/\sigma) \tag{8}$$

where the electric field is

$$\mathbf{E} = \hat{z}\times\nabla_h\partial_t\Psi - \nabla_h(\partial_z\Pi + \mu T)/\mu\sigma + (\nabla_h^2\Pi - \mu\Xi)/\mu\sigma\hat{z} \quad (9)$$

For most of this paper, it will be more convenient to work with the horizontal Fourier transforms of the modal differential equations (7) and (8). The time dependence will be taken as $e^{-i\omega t}$ and the horizontal coordinates transform as

$$\tilde{f}(\eta,\xi) = \int_{-\infty}^{\infty}\int_{-\infty}^{\infty} dxdy\, e^{i(\eta x+\xi y)} f(x,y)$$

$$f(x,y) = \frac{1}{(2\pi)^2}\int_{-\infty}^{\infty}\int_{-\infty}^{\infty} d\eta d\xi\, e^{-i(\eta x+\xi y)}\tilde{f}(\eta,\xi) \quad (10)$$

Let $\hat{z}$ and $\hat{k}$ be unit vectors in the vertical and propagation directions, respectively. The expressions for the magnetic and electric fields (5) and (9) become

$$\tilde{\mathbf{B}} = -ik(\hat{z}\times\hat{k})\tilde{\Pi} - ik\hat{k}\tilde{\Psi} + k^2\tilde{\Psi}\hat{z} \quad (11)$$

and

$$\tilde{\mathbf{E}} = -\omega k(\hat{z}\times\hat{k})\tilde{\Psi} + ik\hat{k}(\partial_z\tilde{\Pi} + \mu\tilde{T})/\mu\sigma - (k^2\tilde{\Pi} + \mu\tilde{\Xi})/\mu\sigma\hat{z} \quad (12)$$

while the differential equations (7) and (8) for the PM and TM modes transform to

$$\partial_z^2\tilde{\Psi} - [k^2 - i\omega\mu\sigma(z)]\tilde{\Psi} = \mu\tilde{Y} \quad (13)$$

and

$$\sigma\partial_z(\partial_z\tilde{\Pi}/\sigma) - [k^2 - i\omega\mu\sigma(z)]\tilde{\Pi} = \mu\tilde{\Xi} - \mu\sigma\partial_z(\tilde{T}/\sigma) \quad (14)$$

where $k=(\eta^2+\xi^2)^{1/2}$ is the magnitude of the horizontal wave number. In addition, continuity of $\tilde{\Psi}$, $\partial_z\tilde{\Psi}$, $\tilde{\Pi}$, and $(\partial_z\tilde{\Pi}+\mu\tilde{T})/\mu\sigma$ is required at horizontal interfaces. The source terms $\tilde{Y}$, $\tilde{\Xi}$, and $\tilde{T}$ in (13) and (14) are discussed in the next section.

Solutions of (13) and (14) are sought for an ocean with vertically varying conductivity $\sigma(z)$ and an arbitrary one-dimensional electrical structure beneath the seafloor. Closed form solution is not tractable, and the approach used in this paper is approximate. Green function solutions to (13) and (14) are constructed for an unbounded ocean of depth H and fixed conductivity equal to that at the seafloor with an arbitrary one-dimensional conducting medium beneath the seafloor, as detailed in Appendix B. The Green functions contain information on the structure of the earth through complex reflection coefficients whose computation for a layered earth model is outlined in Appendix C. These will be useful later in assessing the importance of electromagnetic interactions with the earth. The Green functions may then be used to convert the differential expressions (13) and (14) including vertically varying ocean conductivity into integral equations which completely describe the motional induction problem.

To illustrate, rearrange the terms in (13) to give

$$\partial_z^2\tilde{\Psi} - \beta^2\tilde{\Psi} = \mu\tilde{Y} - i\omega\mu\Delta\sigma(z)\tilde{\Psi} \quad (15)$$

where $\Delta\sigma(z)=\sigma(z)-\sigma(-H)$ and

$$\beta = \sqrt{k^2 - i\omega\mu\sigma(-H)} \quad (16)$$

The PM mode Green function satisfies the left-hand side of (15) with delta function forcing and the relevant boundary conditions, so that (15) may be rewritten as an integral equation. Using the definitions in (12), the result may be expressed in terms of the PM mode electric field

$$\tilde{\mathbf{E}}^{PM}(z) = -\omega\mu k(\hat{z}\times\hat{k})\int_{-H}^{0} dz'\, g_\psi(z,z')\tilde{Y}(z) - i\omega\mu\int_{-H}^{0} dz'\, g_\psi(z,z')\Delta\sigma(z')\tilde{\mathbf{E}}^{PM}(z') \quad (17)$$

This is a second kind integral equation for the spatially Fourier-transformed electric field. The first term on the right side is the primary or driving electric field neglecting interactions of the induced currents with the vertically varying conductivity, while the next term is the secondary electric field due to scattering from the depth-varying conductivity. Equation (17) is similar to those derived for two- or three-dimensional electromagnetic modeling in exploration geophysics [e.g., *Hohmann*, 1983].

Applying Ampere's law, the PM mode horizontal magnetic field follows from (17)

$$\tilde{\mathbf{B}}_h^{PM}(z) = -i\mu k\hat{k}\int_{-H}^{0} dz'\,\partial_z g_\psi(z,z')\tilde{Y}(z') - \mu\hat{z}\times\int_{-H}^{0} dz'\,\partial_z g_\psi(z,z')\Delta\sigma(z')\tilde{\mathbf{E}}^{PM}(z') \quad (18)$$

while the vertical magnetic field satisfies

$$\tilde{B}_z(z) = \mu k^2\int_{-H}^{0} dz'\, g_\psi(z,z')\tilde{Y}(z') + \mu k^2\hat{z}\cdot\left[\hat{k}\times\int_{-H}^{0} dz'\, g_\psi(z,z')\Delta\sigma(z')\tilde{\mathbf{E}}^{PM}(z')\right] \quad (19)$$

The PM mode magnetic field may be regarded as a quantity derived from the electric field, and the interpretation of the right-hand sides of (18) and (19) in terms of primary and secondary components is similar to that for (17).

Proceeding as for the PM mode, the TM mode counterparts of (17)–(19) are a pair of integral equations for the magnetic field and induced electric current density

$$\tilde{\mathbf{B}}^{TM}(z) = -i\mu k(\hat{z}\times\hat{k})\int_{-H}^{0} dz'\, g_\pi(z,z')\tilde{\Xi}(z') - i\mu k(\hat{z}\times\hat{k})\int_{-H}^{0} dz'\,\partial_z g_\pi(z,z')\tilde{T}(z') - \mu\hat{z}\times\int_{-H}^{0} dz'\, g_\pi(z,z')\partial_z\log\sigma(z')\tilde{\mathbf{I}}_h^{TM}(z') - i\omega\mu\int_{-H}^{0} dz'\, g_\pi(z,z')\Delta\sigma(z')\tilde{\mathbf{B}}^{TM}(z') \quad (20)$$

and

$$\tilde{\mathbf{I}}_h^{TM}(z) = ik\hat{k}\int_{-H}^{0} dz'\,\partial_z g_\pi(z,z')\tilde{\Xi}(z') + ik\hat{k}\int_{-H}^{0} dz'\, g_\pi^{+}(z,z')\tilde{T}(z') + \int_{-H}^{0} dz'\,\partial_z g_\pi(z,z')\partial_z\log\sigma(z')\tilde{\mathbf{I}}_h^{TM}(z') - i\omega\hat{z}\times\int_{-H}^{0} dz'\,\partial_z g_\pi(z,z')\Delta\sigma(z')\tilde{\mathbf{B}}^{TM}(z') \quad (21)$$

where $\tilde{\mathbf{I}}_h^{TM}=\sigma\tilde{\mathbf{E}}_h^{TM}$. The first two terms on the right-hand sides

of (20) and (21) are the primary field terms, reflecting the presence of two source terms in (14). The last two terms in (20) and (21) are the secondary field terms due to scattering by the depth-varying seawater conductivity. Finally, using Faraday's law, an expression for the vertical electric field is

$$\tilde{E}_z(z) = \frac{-ik}{\mu\sigma(z)}\hat{z}\cdot\left[\hat{k}\times\tilde{\mathbf{B}}^{TM}(z)\right] - \frac{\tilde{\Xi}(z)}{\sigma(z)} \tag{22}$$

The set of equations (17)–(22) are exact. The form of the integral equations suggests that the motional electromagnetic field is a weighted spatial average of the velocity field with the weighting depending on the Green functions, and hence the conductivity structure below the seafloor, and the vertical distribution of seawater conductivity. In principle, they can be solved for an arbitrary velocity field and conductivity structure by numerical methods using the complete Green function expressions of Appendix B, although such an approach is unlikely to be enlightening in terms of the relevant physics.

THE LOW FREQUENCY, LARGE SCALE APPROXIMATION

The interaction of the electromagnetic and hydrodynamic fields is complex, as evidenced by the form of (17)–(22) and previous treatments such as that of *Sanford* [1971]. However, some properties of the real ocean at subinertial frequencies may be used to simplify the mathematical expressions and delve into the underlying physics, including (1) the horizontal length scale of motion is typically larger than the vertical one by a factor of 10 or more, and (2) the vertical velocity is generally small compared to the horizontal components. In the spatial Fourier domain, the first of these is the condition $kH \ll 1$. The remaining constraint is applied in Appendix D during derivation of expressions for the source terms $\tilde{\mathbf{Y}}$, $\tilde{\Xi}$, and $\tilde{\mathbf{T}}$.

In the integral equations (17)–(22), kH enters through the exponential terms in the Green functions given in Appendix B. These terms contain arguments of the form βz, $-H \le z \le 0$, where β in (16) parameterizes the effect of self induction in seawater. To derive approximate forms for the Green functions using a first-order Taylor series expansion on the exponential terms, it is necessary to require that $|\beta H| \ll 1$; this is equivalent to placing an additional constraint on the extent of self induction. To see this, define the dimensionless induction or magnetic Reynolds number

$$\varepsilon = \frac{\omega\mu\sigma(-H)}{2k^2} \tag{23}$$

so that

$$|\beta H| = kH\,|\sqrt{1-i2\varepsilon}\,| \tag{24}$$

The induction number is the ratio of the squares of the hydrodynamic and electromagnetic length scales; when it is small, the latter is large compared to the former and induction is not important, so the system displays only simple electric dissipation without large phase shifts. For (24) to be small, $|(1-i2\varepsilon)^{1/2}|$ must be O(1) or less, or ε must itself be O(1) or below. For a crude estimate of the size of the induction number, consider two prototypical subinertial flows, an external mode Rossby wave at mid-latitudes with characteristic period T=O(10 d) and wavelength L=O(1000 km) and mesoscale eddy motions with T=O(100 d), L=O(100 km). In the first instance, (23) gives an induction number of 0.4, while in the second case it is only 4×10^{-4}. These types of motions will satisfy the condition on (24) without difficulty. However, for large-scale motions at relatively high frequencies, breakdown may occur. For example, in the basin-wide oscillation detected by *Luther* [1982] with T=O(5 d), L=O(10000 km) the induction number is about 75. Note also that the tides violate the induction number criterion; a diurnal coastal Kelvin wave has $\varepsilon \approx 800$, so induction effects are quite large.

It is also necessary to examine the behavior of the reflection coefficients to simplify the Green functions in (17)–(22). Consider a simple model consisting of an ocean layer of conductivity $\sigma(-H)$ overlying a half-space of conductivity σ_l. The PM mode sea surface and seafloor reflection coefficients and the TM mode seafloor reflection coefficient given in Appendix B may be written

$$R_A^{PM} = \frac{\sqrt{1-i2\varepsilon} - 1}{\sqrt{1-i2\varepsilon} + 1} \tag{25}$$

$$R_L^{PM} = \frac{\sqrt{1-i2\varepsilon} - \sqrt{1-i2\kappa\varepsilon}}{\sqrt{1-i2\varepsilon} + \sqrt{1-i2\kappa\varepsilon}} \tag{26}$$

$$R_L^{TM} = \frac{\kappa\sqrt{1-i2\varepsilon} - \sqrt{1-i2\kappa\varepsilon}}{\kappa\sqrt{1-i2\varepsilon} + \sqrt{1-i2\kappa\varepsilon}} \tag{27}$$

where $\kappa = \sigma_l/\sigma(-H)$ and ε is the induction number (23). Since $\kappa \ll 1$, when ε is small the PM mode reflection coefficients (25) and (26) are also small and nearly imaginary; they become real and approach a magnitude of 1 for large induction numbers, but more typically lie between 0.6 and 0.9 in absolute value. However, the TM mode reflection coefficient (27) behaves in a very different way. In the small induction number limit it is almost -1 and remains very close to that value throughout the parameter range of interest. The TM mode transmission coefficient is defined as

$$T_L^{TM} = 1 + R_L^{TM} \tag{28}$$

This is nearly real and has a magnitude that may be comparable to that of (24). For this reason, both (24) and (28) will be treated as small parameters in the remainder of the paper.

Using these results, the PM mode Green function and its vertical derivative given in Appendix B are approximated for $kH \ll 1$ and induction number O(1) or less by expanding the exponential terms in the numerator and denominator in Taylor series. Retaining only the lowest order terms, this gives

$$g_\psi(z,z') = f_\psi \approx -\frac{(R_A^{PM}+1)(R_L^{PM}+1)}{2\beta(1-R_A^{PM}R_L^{PM})} \tag{29}$$

$$\partial_z g_\psi(z,z') = h_\psi \approx \frac{(R_A^{PM}+1)(R_L^{PM}-1)}{2(1-R_A^{PM}R_L^{PM})} \quad (z<z')$$

$$= h_\psi + 1 \qquad (z>z') \tag{30}$$

The first of these is depth-independent, while the second undergoes a unit step change at $z=z'$.

For the TM mode, the Green function and its derivatives given in Appendix B may be approximated

$$g_\pi(z,z') \approx \tfrac{1}{2}(1-h_\pi H)(|z-z'|+z+z') \tag{31}$$

$$\partial_z g_\pi(z,z') \approx h_\pi z' \qquad (z<z')$$

$$\approx h_\pi z' + 1 \quad (z>z') \tag{32}$$

$$\partial_{z'} g_\pi(z,z') \approx h_\pi z + 1 \quad (z<z')$$

$$\approx h_\pi z \qquad (z>z') \tag{33}$$

$$\partial_z \partial_{z'} g_\pi(z,z') = g_\pi^+(z,z') - \delta(z-z') \approx h_\pi - \delta(z-z') \quad (34)$$

where

$$h_\pi = \frac{\beta(2-T_L^{TM})}{T_L^{TM} - 2R_L^{TM}\beta H} \quad (35)$$

and δ is the Dirac delta function. The expressions (29)–(35) are valid to terms of $O(|\beta H|)$ and have been verified numerically. The use of these approximations in (17)–(22) formally requires that the principal contribution to the inverse Fourier transform in (10) be from small wave numbers where the velocity is significant and is equivalent to replacing the infinite integration limits by a cutoff wave number k_c which is not well defined, but $O(1/H)$. Note that (29) and (34), which appear in the expressions for the horizontal electric and vertical magnetic fields, are depth-independent, while (30) and (33), which appear in the expressions for the horizontal magnetic field, undergo a step change within the water column. The former are consistent with intuition about low-frequency induction in the ocean, but the integral equation expressions in (17)–(22) are actually more complicated than this due to the secondary field terms and depth-varying conductivity.

The source terms $\tilde{Y}$, $\tilde{T}$, and $\tilde{\Xi}$ in (13)–(14) and (17)–(22) are given by the Fourier transforms of Poisson equations derived in Appendix A and the vertical component of the source current density. To simplify these equations, some properties of the real geomagnetic field must be considered. In Appendix D, an inclined geocentric dipole model for the geomagnetic field is used to get an approximation valid for mid-latitudes under the assumption that the vertical velocity is small compared to the horizontal ones. Taking Fourier transforms and neglecting terms involving the spatial variation of the geomagnetic field gives

$$\tilde{\Xi}(z) = \sigma(z)[\tilde{\mathbf{v}}_h(z) \times \tilde{\mathbf{F}}_h^o] \quad (36)$$

$$\tilde{T}(z) = \frac{i\sigma(z)}{k}[\hat{k} \times \tilde{\mathbf{v}}_h(z)] \cdot F_z^o \hat{z} \quad (37)$$

$$\tilde{Y}(z) = -\frac{i\sigma(z)}{k}[\hat{k} \cdot \tilde{\mathbf{v}}_h(z)] F_z^o \quad (38)$$

where $\mathbf{F}^o$ is the geomagnetic induction at a reference latitude λ_o and longitude ϕ_o. Note that (37) and (38) contain the Fourier transforms of the vertical component of relative vorticity and the horizontal divergence of the horizontal water velocity, and drive the TM and PM modes, respectively, in (17)–(22). For a graphical view of this association, see Figure 1.

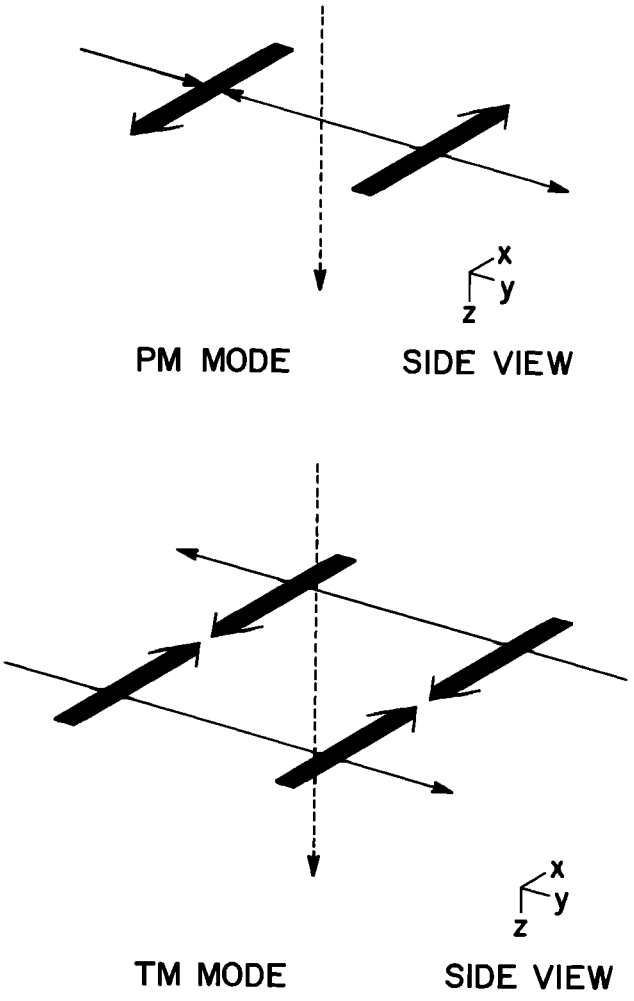

Fig. 1. Cartoon showing the modal source mechanisms for low-frequency, large-scale oceanic flows. The dashed line shows the vertical component of the geomagnetic field, while the solid line denotes the water velocity, and the double line is the source emf. The top part of the figure depicts a side view of a velocity field with horizontal divergence, such as occurs in gravity waves with displacement of the sea surface. The source currents flow in horizontal loops in alternate directions along peaks and troughs of the wave, closing at infinity. The bottom part of the figure shows a plan view of a velocity field with relative vorticity. The induced electric currents are horizontally divergent, cannot penetrate the sea surface because the atmosphere is insulating, and so dive down into the earth over horizontal distances comparable to that of the velocity field.

APPROXIMATE PM MODE SOLUTION

The integral equation for the PM mode electric field (17) is combined with the approximate Green function (29) and the source term (38) to give

$$\tilde{E}^{PM}(z) + i\omega\mu f_\psi \int_{-H}^{0} dz' \, \Delta\sigma(z) \tilde{E}^{PM}(z')$$

$$= i\omega\mu \langle\sigma\rangle H F_z^o f_\psi (\hat{k} \cdot \langle\tilde{\mathbf{v}}_h\rangle^*) \quad (39)$$

where $\langle\sigma\rangle$ is the depth-averaged conductivity of seawater

$$\langle\sigma\rangle = \frac{1}{H}\int_{-H}^{0} dz' \, \sigma(z') \quad (40)$$

and $\langle\tilde{\mathbf{v}}_h\rangle^*$ is the vertically-integrated, conductivity-weighted horizontal water velocity

$$\langle\tilde{\mathbf{v}}_h\rangle^* = \frac{1}{\langle\sigma\rangle H}\int_{-H}^{0} dz' \, \sigma(z') \tilde{\mathbf{v}}_h(z') \quad (41)$$

The definition in (41) reduces to the depth-averaged (barotropic) one if the velocity field or conductivity is depth-independent. Expression (39) is a simple Fredholm integral equation with a degenerate kernel and can be reduced to an algebraic equation by standard methods. The solution is

$$\tilde{E}^{PM} = \frac{i\omega\mu\langle\sigma\rangle H F_z^o f_\psi (\hat{k} \cdot \langle\tilde{\mathbf{v}}_h\rangle^*)}{1 + i\omega\mu(\langle\sigma\rangle - \sigma(-H))H f_\psi}$$

$$\approx i\omega\mu\langle\sigma\rangle H F_z^o f_\psi (\hat{k} \cdot \langle\tilde{\mathbf{v}}_h\rangle^*) \quad (42)$$

where the second form is obtained by neglecting small terms and is just the primary field in (17). The PM mode electric field is in the horizontal plane and orthogonal to the direction of propagation for the velocity field.

The PM mode horizontal magnetic field follows from (18) with the approximate Green function (30), the source term (38), and (42). Neglecting small terms, the result is

$$\tilde{B}_h^{PM}(z) = -\mu<\sigma>F_-^o\,\hat{k}\cdot\left[h_\psi H<\tilde{\mathbf{v}}_h>^* + (z+H)<\tilde{\mathbf{v}}_h>_{-H}^{-}\right] \quad (43)$$

where

$$<\tilde{\mathbf{v}}_h>_{-H}^{-} = \frac{1}{<\sigma>(z+H)}\int_{-H}^{-} dz'\,\sigma(z')\,\tilde{\mathbf{v}}_h(z') \quad (44)$$

so that $<\tilde{\mathbf{v}}_h>_{-H}^{0} = <\tilde{\mathbf{v}}_h>^*$. Expression (43) is depth-dependent, and the second term vanishes at the seafloor. The PM mode horizontal magnetic field is oriented in the direction of propagation for the velocity field.

The vertical magnetic field is depth-independent and follows from a similar calculation with (19), giving

$$\tilde{B}_- = -i\mu<\sigma>kHF_-^o f_\psi\,\hat{k}\cdot<\tilde{\mathbf{v}}_h>^* \quad (45)$$

Approximate TM Mode Solution

The integral equations for the TM mode horizontal electric current density and magnetic fields (20) and (21) are a coupled set and should be solved simultaneously. To simplify and decouple them, the motional magnetic field will be assumed small enough that its contribution to (21) is negligible and a solution for the induced electric current density at lowest order will be obtained. This will be used in (20) to get the motional magnetic field, and substituted back into (21) to get a better estimate of the current density. This iterative procedure ends when the new terms are small in the usual sense.

It is first necessary to simplify the primary part of (21) since there are two sources, the vertical source current (36) and the scalar representing the horizontally divergent part of the horizontal source current (37). Substituting the Green functions (32) and (34) and the source terms (36) and (37) gives a sum of three terms. Hölder's inequality may be used to bound and compare their magnitudes. Such an analysis shows that the two terms from the vertical source current (36) are similar in magnitude but simultaneously $O(kH\,|\,F_\psi^o/F_-^o\,|\,)$ compared to that from (37). The horizontal current term is dominant except near the magnetic equator where F_-^o vanishes. That vertical source currents are not efficient at inducing electric currents in the ocean is not surprising; vertical sources have a scale like that of the water column, while horizontal sources have a scale comparable to that of the hydrodynamic field and hence are better able to induce horizontal currents in the ocean and earth. At middle to high latitudes, the primary induced electric current density is well approximated by

$$\tilde{I}_{h,(0)}^{TM} = -<\sigma>h_\pi HF_-^o\,(\hat{k}\times<\tilde{\mathbf{v}}_h>^*)\cdot\hat{z} \quad (46)$$

The next order approximation to the electric current density satisfies the integral equation

$$\tilde{I}_{h,(1)}^{TM}(z) - \int_{-H}^{-} dz'\,\partial_{z'}\log\sigma(z')\,\tilde{I}_{h,(1)}^{TM}(z') = \tilde{I}_{h,(0)}^{TM} + h_\pi\int_{-H}^{0} dz'\,z'\,\partial_{z'}\log\sigma(z')\,\tilde{I}_{h,(1)}^{TM}(z') \quad (47)$$

The right side of (47) is an unknown constant, and a Neumann series solution to the remaining Volterra integral equation in terms of this constant can easily be constructed. The remaining problem reduces to the solution of an algebraic equation, yielding

$$\tilde{I}_{h,(1)}^{TM}(z) = \frac{\tilde{I}_{h,(0)}^{TM}\sigma(z)}{\sigma(-H) + h_\pi H(<\sigma> - \sigma(-H))} \quad (48)$$

Note that the electric field corresponding to (48) is depth-independent while that for the primary term (46) is not, and that the new term obtained by solving (47) is not small.

The lowest-order approximation for the TM mode magnetic field from (20) is given by the sum of the first three terms after applying (31), (33), (35)-(37), and (48). As for the induced electric current (46), it can be shown that the contribution due to the vertical source current is negligible compared to that from the horizontally divergent part of the source current, yielding

$$\tilde{B}_{(0)}^{TM}(z) = \mu<\sigma>F_-^o\,\hat{k}\times\left[\left[H\sigma(-H)(1-h_\pi H) + h_\pi H\left[h_\pi H(z+H)<\sigma> + (1-h_\pi H)\int_{-H}^{-} dz'\,\sigma(z')\right]\right]<\tilde{\mathbf{v}}_h>^* / \left[\sigma(-H) + h_\pi H(<\sigma> - \sigma(-H))\right] - (z+H)<\tilde{\mathbf{v}}_h>_{-H}^{-}\right]\cdot\hat{z} \quad (49)$$

Note that this vanishes at $z=0$, as expected for the TM mode magnetic field.

The next order approximation for the magnetic field follows by substituting the Green function (31) into the last term in (20), yielding the integral equation

$$\tilde{B}_{(1)}^{TM}(z) + i\omega\mu(1-h_\pi H)\int_{-H}^{-} dz'\,(z-z')\,\Delta\sigma(z')\,\tilde{B}_{(1)}^{TM}(z) = \tilde{B}_{(0)}^{TM}(z) - i\omega\mu(1-h_\pi H)\int_{-H}^{0} dz'\,z'\,\Delta\sigma(z')\,\tilde{B}_{(1)}^{TM}(z') \quad (50)$$

As in (47), the right-hand side of (50) is an unknown constant, and the Volterra part of the integral equation may be solved by constructing a Neumann series for the equivalent resolvent equation. This gives a convergent series whose entries are each $O[(kH)^2]$ compared to the previous one, and the first term alone is a satisfactory approximation. Using this, the second term in (50) is seen to be $O[(kH)^2]$ compared to (49) and may be neglected. In a similar way the last term in (50) is also found to be small, and (49) is a consistent expression for the motional magnetic field.

Returning to the induced electric current integral equation (21), it is now possible to evaluate the contribution from the secondary magnetic field given by the last term with (49). This term is $O[(kH)^2]$ compared to (48), so the coupling between the integral equations (20) and (21) is weak. Similarly, the third term in (20) does not contribute significantly to the motional magnetic field, and the approximate procedure used to get a solution is justified.

Finally, the vertical electric field follows from (22) with (36) and (49). Applying Hölder's inequality once again, the ratio of the first to the second term is seen to be $O(kH\,|\,1-h_\pi H\,|\,\,|\,F_-^o\,|\,/\,|\,F_h^o\,|\,)$. This is typically $O(kH)$ away

from the poles, so the vertical electric field is very nearly equal to

$$\tilde{E}_z = -(\tilde{\mathbf{v}}_h(z)\times\tilde{\mathbf{F}}_h^o)\cdot\hat{z} \tag{51}$$

This result is the wave number domain counterpart to that given by *Harvey* [1974]. The vertical electric field is independent of the electrical structure of the earth because vertical electric currents cannot readily penetrate the relatively poorly conducting earth and nearly insulating atmosphere.

THE ELECTROMAGNETIC FIELDS IN THE WAVE NUMBER DOMAIN

While the PM and TM modes provide both a physical view of the induction process and a substantial mathematical simplification, they cannot be measured independently, and the separate expressions for the horizontal electric and magnetic fields must be combined. For the horizontal electric component, the relevant expressions are given by (42) and the induced current density (48) divided by the in situ conductivity of seawater. The result can be simplified using the identity $\hat{k}\,[\hat{k}\times\langle\tilde{\mathbf{v}}_h\rangle^*]\cdot\hat{z} = -\hat{z}\times\langle\tilde{\mathbf{v}}_h\rangle^* + (\hat{z}\times\hat{k})\hat{k}\cdot\langle\tilde{\mathbf{v}}_h\rangle^*$. Neglecting the PM mode term that is $O(kH)$ compared to the TM mode contributions, the horizontal electric field is given by

$$\tilde{\mathbf{E}}_h = \tilde{\Gamma}\,F_z^o\,\hat{z}\times\left[\langle\tilde{\mathbf{v}}_h\rangle^* - \hat{k}\,\hat{k}\cdot\langle\tilde{\mathbf{v}}_h\rangle^*\right] \tag{52}$$

where

$$\tilde{\Gamma} = \frac{\langle\sigma\rangle h_\pi H}{\sigma(-H) + h_\pi H(\langle\sigma\rangle - \sigma(-H))} \tag{53}$$

is a dimensionless function. The electric field is depth-independent and consists of two parts. The first term is due to direct forcing by the velocity field, while the second one is related to large-scale horizontal velocity divergence and will be discussed later. The electric field is proportional to a factor (53) which is dependent on wave number, frequency, and the electrical structures of the ocean and earth, and contains all of the essential information on the leakage of electric current into the conducting earth that determines the size of (52). This term is nearly real and has a magnitude which lies between 0 and 1 as the earth ranges from a good conductor to a perfect insulator. Note that (53) is a generalization of simpler calculations given by *Sanford* [1971] and *Cox* [1981].

The horizontal magnetic field is given by the sum of (43) and (49). Unlike the horizontal electric field, the motional magnetic field is markedly depth-dependent. Because vector magnetic field sensors are extremely sensitive to motion in the geomagnetic field, it is not feasible to measure magnetic components except at the seafloor, and only that location will be considered further. The result can be simplified using the identity $(\hat{z}\times\hat{k})\,[\hat{k}\times\langle\tilde{\mathbf{v}}_h\rangle^*]\cdot\hat{z} = \langle\tilde{\mathbf{v}}_h\rangle^* - \hat{k}(\hat{k}\cdot\langle\tilde{\mathbf{v}}_h\rangle^*)$ to give

$$\tilde{\mathbf{B}}_h(-H) = \mu\langle\sigma\rangle H F_z^o\left[(1-\tilde{\Gamma})\langle\tilde{\mathbf{v}}_h\rangle^* - \hat{k}(1-\tilde{\Gamma}+h_\psi)\,\hat{k}\cdot\langle\tilde{\mathbf{v}}_h\rangle^*\right] \tag{54}$$

The balance of terms in (54) is not nearly as straightforward as in (52) and requires careful examination of (30) and (53) as a function of frequency and wave number for realistic earth models. However, the sensitivity of the magnetic field to the earth's conductivity has the opposite sense to (52) since a poorly conducting earth results in $1-\tilde{\Gamma}\approx 0$. This is intuitively reasonable because image currents in the earth result in reinforcement of the seafloor horizontal magnetic field and are weak in the presence of resistive material. Equations (52) and (54), together with (45) and (51), are wave number domain expressions valid in the low-frequency, large-scale limit when induction is not large.

INTERACTIONS OF MOTIONAL FIELDS WITH THE EARTH

Interactions of motional electromagnetic fields with the conducting ocean and earth are described by the term (53) which appears in both (52) and (54) and by (30). Understanding the influence of these regions requires a geophysically reasonable model for the electrical conductivity structures of both the oceans and earth.

Precise empirical relationships between seawater conductivity and its temperature, salinity, and pressure exist [e.g., *Fofonoff and Millard*, 1983] and may be used to compute seawater conductivity using temperature and salinity profile data. The dominant effect is due to temperature, although rising pressure typically results in a small increase in conductivity near the seafloor. Figure 2 shows such a calculation using historic 5° zonal averages of potential temperature (converted to in situ temperature) and salinity at 42.5°N in the Pacific taken from *Levitus* [1982]. Most of the change in conductivity occurs above the main thermocline, and the conductivity is nearly constant below that point. The depth-averaged conductivity $\langle\sigma\rangle$ for this profile is 3.18 S/m, about 2% smaller than the seafloor value $\sigma(-H)$ of 3.25 S/m.

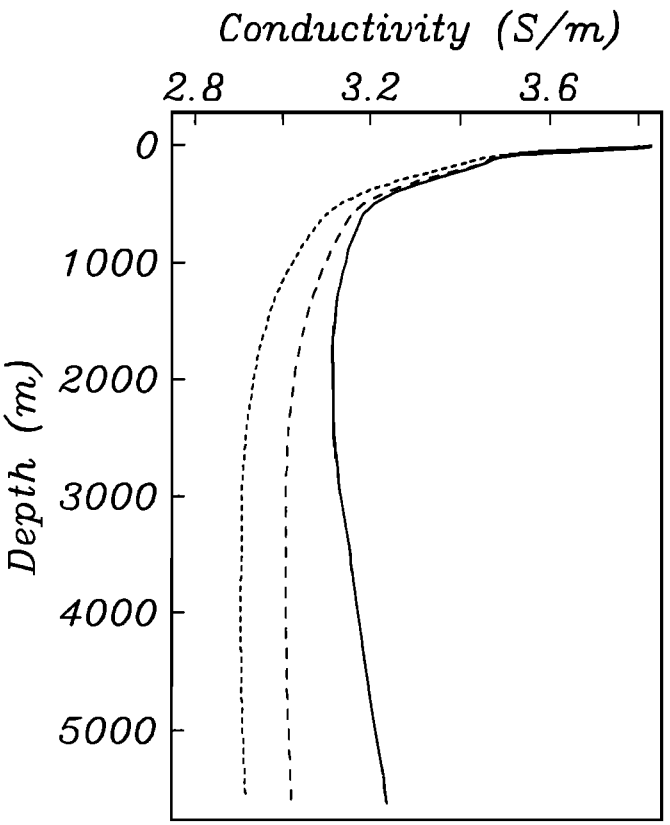

Fig. 2. Profile of the electrical conductivity of seawater computed from the empirical formulae given by *Fofonoff and Millard* [1983] using 5° zonal averages of the potential temperature (converted to in situ temperature) and salinity from *Levitus* [1982]. The short-dashed line includes the temperature dependence only and assumes a constant salinity of 33.4 ppt and zero pressure. The long-dashed line adds the real salinity dependence to the computation. The solid line is the full treatment including the pressure dependence of conductivity.

A reference model for the electrical structure beneath the deep seafloor has recently been proposed by *Chave et al.* [1990] based on a variety of geophysical and geochemical data. It can be divided into three main regions: sediments, crust, and mantle. The thickness and conductivity of the sedimentary region is highly variable in space. It nearly vanishes in much of the Pacific and can be 1 km or more thick in the Atlantic Ocean, so the model is subdivided into two types. In the Pacific model, no sediment is included, while in the Atlantic model, a 0.5 km thick sedimentary zone of conductivity 0.3 S/m is added. The oceanic crust is about 6.5 km thick and consists of a 0.6 km upper zone of conductivity ≈0.03 S/m overlying a 5.9 km lower region of conductivity ≈0.003 S/m. Beneath this point, the conductivity falls sharply to a value of $\approx 10^{-5}$ S/m over a distance of 30 km; the presence of a resistive zone beneath the crust is supported by controlled source electromagnetic soundings reported by *Cox et al.* [1986]. Below this region, the conductivity must rise rapidly due to increasing temperature. This is simulated by a 40 km thick zone of conductivity 0.003 S/m overlying a 0.1 S/m half-space. The reference model is believed to be generally valid away from coastlines and mid-ocean spreading centers; for a justification see *Chave et al.* [1990]. Figure 3 summarizes the Pacific and Atlantic conductivity models.

Figure 4 shows a contour plot of (53) as a function of frequency in cycles per hour and inverse wavelength in cycles per kilometer using the Pacific reference model and the seawater conductivity profile of Figure 2. The frequency scale covers the range of 10^{-4}–10^{-1} cph (10 hours to 1 year period), while a useful range for the inverse wavelength is 5×10^{-4} cpkm (Pacific basin scale) to 5×10^{-2} cpkm (submesoscale). The magnitude of (53) is almost frequency-independent, reflecting the small size of the induction number, and nearly a constant function of the inverse wavelength, varying from more than 0.9 to almost 1 over the relevant range. Its phase is nearly zero, reflecting the smallness of induction. Figure 5 shows similar calculations for the Atlantic conductivity model. The sedimentary layer produces a slight reduction in the magnitude of (53),

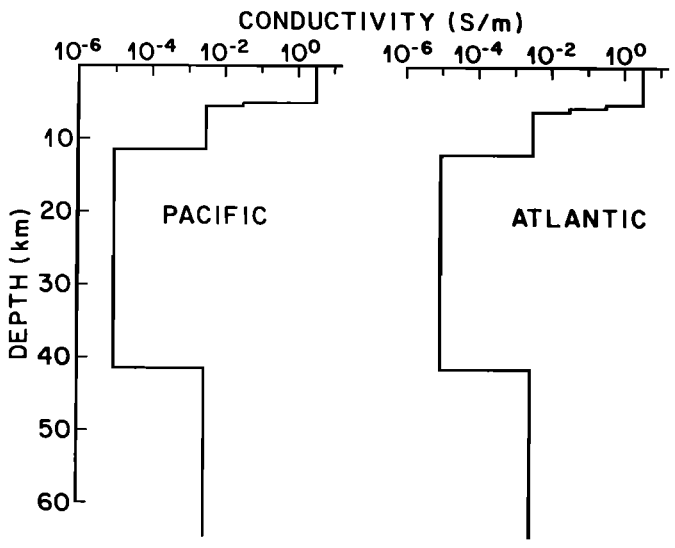

Fig. 3. The Pacific (left) and Atlantic (right) reference models for the conductivity structure beneath the ocean as given by *Chave et al.* [1990]. The two differ by the presence of a thin (≈0.5 km) layer of relatively conductive sediment in the Atlantic model. Both models are terminated in a half-space of conductivity 0.1 S/m below 71 km depth.

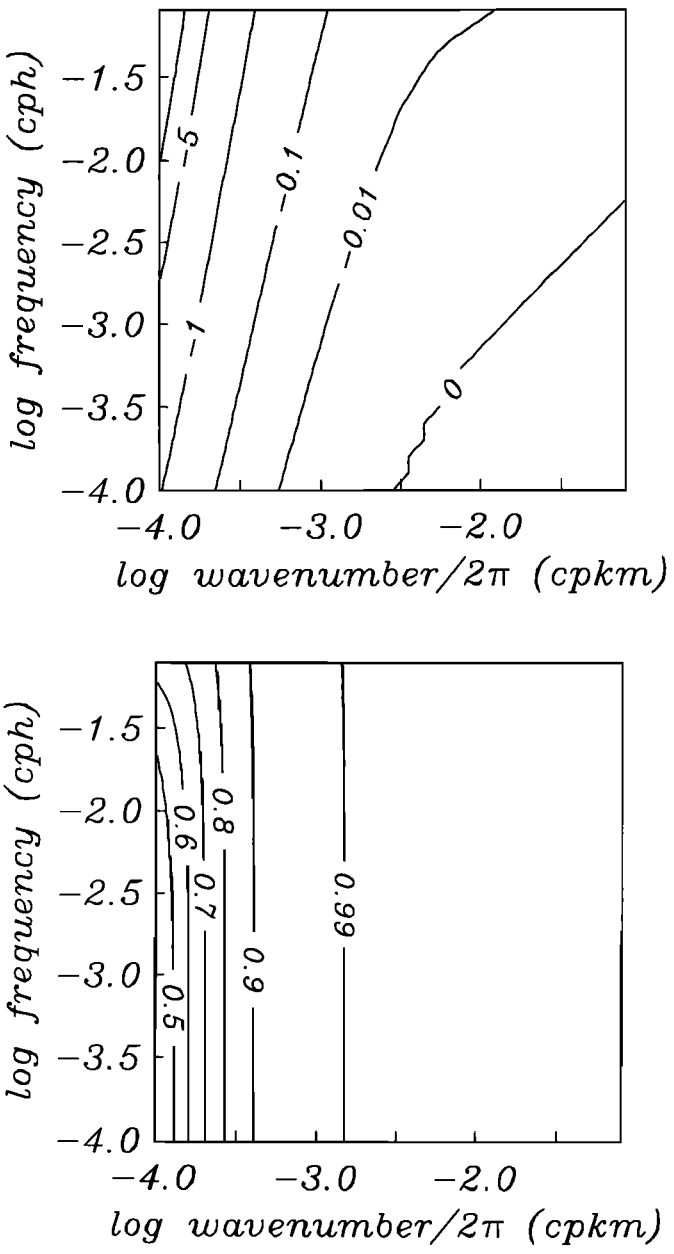

Fig. 4. Contour plots of the magnitude (bottom) and phase in degrees (top) of Γ given by (53) in the text as a function of frequency and inverse wavelength using the Pacific reference model of Figure 3.

especially at small values of the inverse wavelength, but it remains nearly frequency-independent and real. These observations are not changed, except at the largest spatial scales, if the conductivity of the resistive mantle region is raised by a decade (Figure 6). The behavior of (53) is controlled mostly by the presence of a relatively conductive sediment and crustal zone and a nearly insulating cap beneath it, and is quite insensitive to the conductivity of the deeper mantle. In the absence of a crustal zone, the response is almost that of an insulating half-space with a magnitude of 1 at all frequencies and wavelengths. If the insulating region is not present, the electric field is effectively shorted out beginning with the longest wavelength components, and (48) becomes very small. This behavior begins to be evident in Figure 6. Computations like

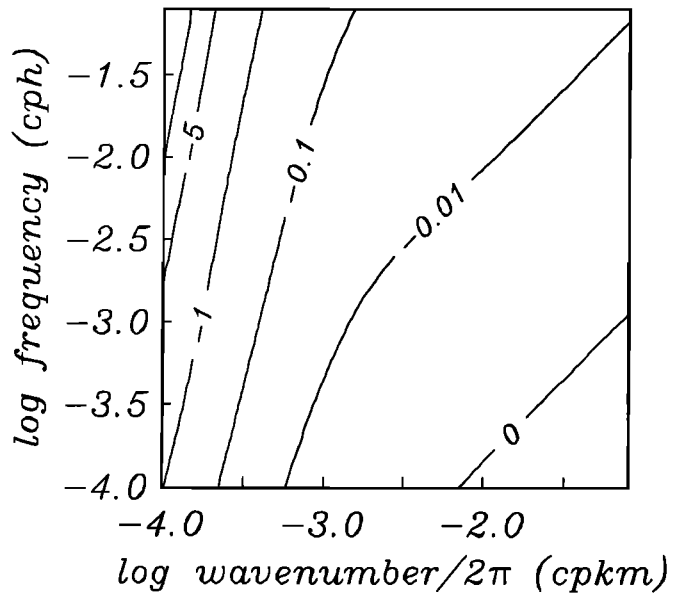

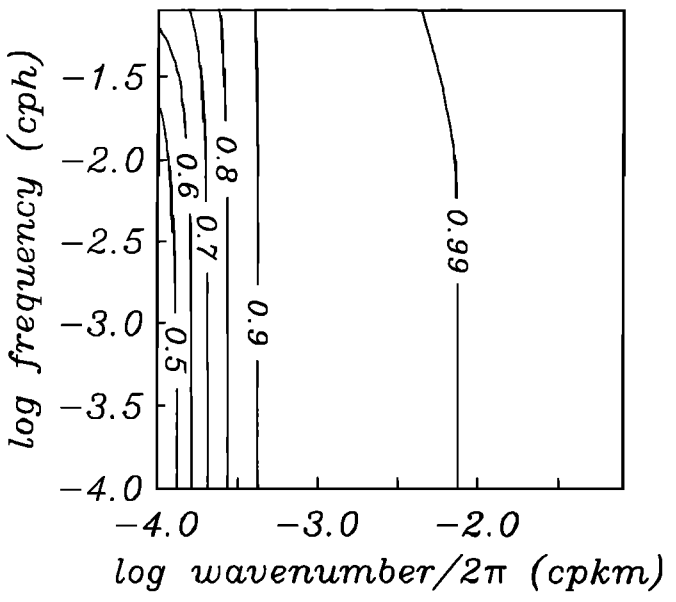

Fig. 5. Contour plots of the magnitude (bottom) and phase in degrees (top) of $\tilde{\Gamma}$ given by (53) in the text as a function of frequency and inverse wavelength using the Atlantic reference model of Figure 3.

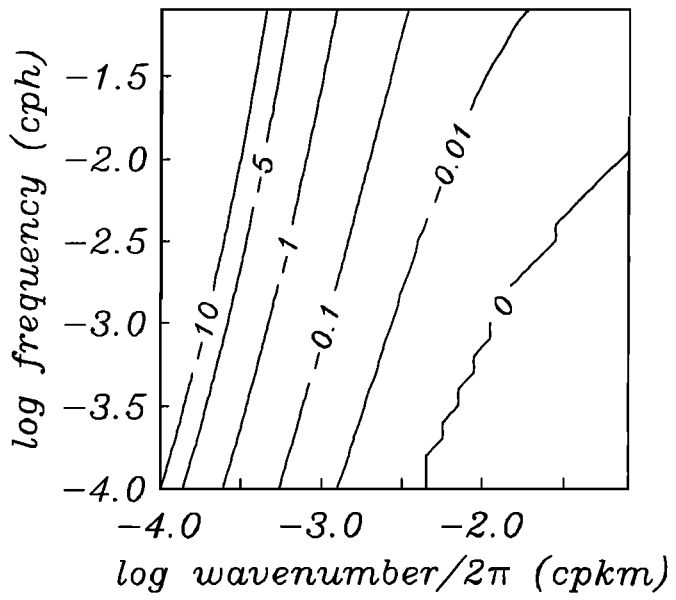

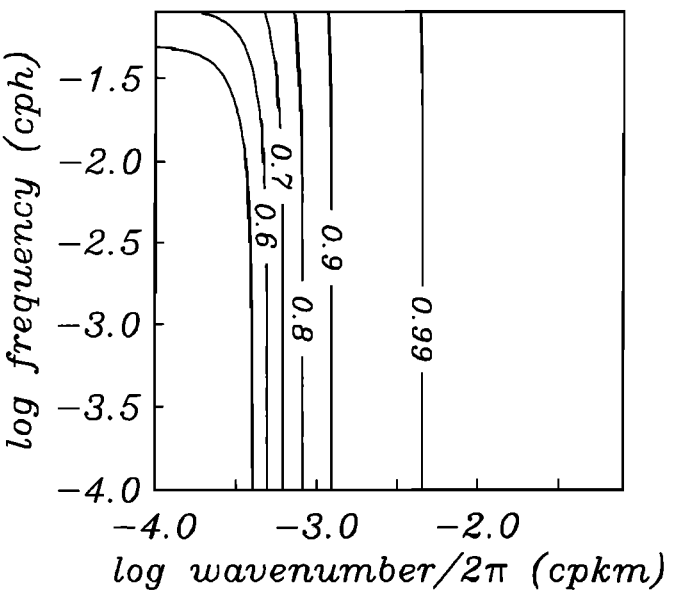

Fig. 6. Contour plots of the magnitude (bottom) and phase in degrees (top) of $\tilde{\Gamma}$ given by (53) in the text as a function of frequency and inverse wavelength using the Pacific reference model of Figure 3 but with the subcrustal layer conductivity increased to 10^{-4} S/m.

those for Figures 4–6 are also relatively insensitive to the seawater conductivity profile and the comparative sizes of $<\sigma>$ and $\sigma(-H)$.

The seafloor horizontal magnetic field (54) is a balance between two terms. The former is scaled by $1-\tilde{\Gamma}$ which is nearly zero over the entire subinertial range of frequency and inverse wavelength from Figures 4–6. The second term contains an additional factor h_ψ in the proportionality constant which is very nearly −0.5 throughout the subinertial range. The factor $1-\tilde{\Gamma}+h_\psi$ is not small, so the balance between the two terms in (54) depends heavily on their actual size and behavior in the space domain.

THE ELECTROMAGNETIC FIELDS IN THE SPATIAL DOMAIN

Space domain expressions for the horizontal electric and magnetic fields formally follow by applying the inverse Fourier transform (10) with integration limits k_c to (52) and (54). These require a spatial convolution relationship between averaging kernels obtained from the inverse transform of linear operations on (53) and the vertically-integrated, conductivity-weighted horizontal water velocity. The spatial behavior of the averaging kernels will be examined as a guide to interpretation of motional electromagnetic fields. Since the cutoff wave number k_c is not precisely defined and (53) is only approximate, precise details of the averaging kernel behavior are not important. In particular, the physical width of the main lobe and extent of leakage from sidelobes should not be emphasized; rather, it is the general shape and spatial averaging properties that are of direct interest. Based on the properties of solutions to the complete integral equations (17)–(21) at all wave numbers, the approximate kernels given below serve only as upper bounds with wider spatial breadths and larger sideband amplitudes than will really occur.

Performing the integration (10) on (52) yields

$$\mathbf{E}_h = CF_-^o \hat{z} \times \left[\Omega_1 \oplus <\mathbf{v}_h>^* + \nabla_h \Omega_2 \oplus \nabla_h \cdot <\mathbf{v}_h>^*\right] \quad (55)$$

where Ω_1 is the inverse Fourier transform of $\tilde{\Gamma}/C$, $\nabla_h\Omega_2$ is the horizontal gradient of the inverse Fourier transform of $\tilde{\Gamma}/Ck^2$, C is a constant, and $\oplus$ denotes convolution over the horizontal spatial coordinates. Equation (55) is simpler than it initially appears, as can be seen by using the results of the last section to approximate $\tilde{\Gamma}$ as a constant C independent of wave number. This gives

$$\Omega_1(\rho) \approx \frac{k_\epsilon}{\sqrt{2}\pi} \frac{J_1(\sqrt{2}k_\epsilon\rho)}{\rho} \quad (56)$$

and

$$\nabla_h\Omega_2(\rho) \approx \frac{\nabla_h\rho}{2\pi\rho}\left[J_0(\sqrt{2}k_\epsilon\rho) - 1\right] \quad (57)$$

where J_0 and J_1 are Bessel functions of the first kind. Figure 7 shows (56), while Figure 8 shows expression (57) divided by the angular factor $\nabla_h\rho=(\cos\theta,\sin\theta)$. Equation (56) is the two-dimensional analog of the sinc function. It is sharply peaked at the origin with a main lobe of width $\approx 2.8/k_\epsilon$ and sidelobes which fall off quickly with range. This means that the first term of (56) is a spatial average of the vertically-integrated, conductivity-weighted horizontal water velocity with a horizontal averaging scale of order a few times the water depth or less. The second term in (55) is a spatial average of the horizontal divergence of the conductivity-weighted, vertically-integrated water velocity. The averaging kernel possesses double dipolar symmetry because of the $\nabla_h\rho$ term, vanishes at the origin, peaks several times the water depth away from it, and falls off slowly with range relative to (56) as seen in Figure 8. This yields a nonlocal average of $\nabla_h\cdot<\mathbf{v}_h>^*$; because of the dipolar symmetry its value will nearly be zero unless that quantity changes rapidly with range and possesses marked azimuthal asymmetry. Since $|\nabla_h\cdot<\mathbf{v}_h>^*| \le \sigma(0)|w(0)|/<\sigma>H$, where w(0) is the surface vertical velocity, the ratio of the second to the first term in (55) is small even in the absence of azimuthal averaging.

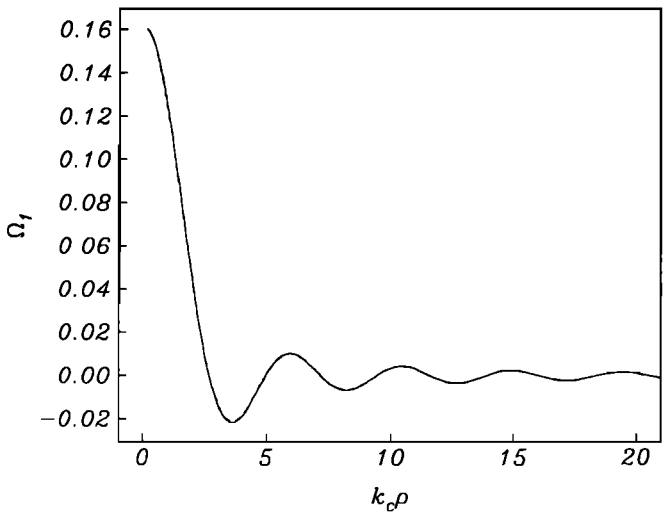

Fig. 7. Approximate form of the horizontal electric field averaging kernel given by (56) in the text which serves as a gross limit to the real averaging function. The abscissa shows horizontal distance in units of k_ϵ^{-1} which is of order units of water depths.

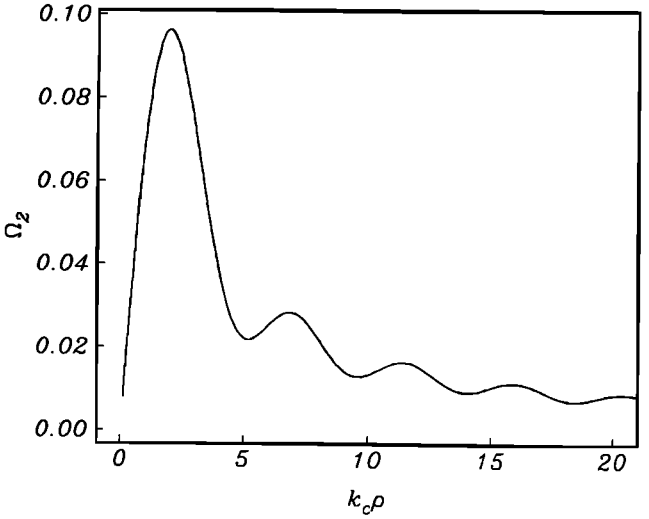

Fig. 8. Approximate form of the horizontal electric field averaging kernel given by (57) in the text divided by the angular factor $\nabla_h\rho$. The abscissa shows horizontal distance in units of k_ϵ^{-1} which is of order units of water depths.

Approximating $h_\psi \approx -0.5$ and proceeding as for (55), the horizontal magnetic field (54) becomes

$$\mathbf{B}_h(-H) = \mu<\sigma>F_-^o H\left[\Omega_3 \oplus <\mathbf{v}_h>^* + \nabla_h\Omega_4 \oplus \nabla_h\cdot<\mathbf{v}_h>^*\right] \quad (58)$$

where Ω_3 is the inverse Fourier transform of $1-\tilde{\Gamma}$ and $\nabla_h\Omega_4$ is the horizontal gradient of the inverse Fourier transform of $(\tilde{\Gamma}-0.5)/k^2$. The behavior of the averaging kernels in (58) is very different from that in (55). From Figures 4–6, $1-\tilde{\Gamma}$ is nearly 1 for wave numbers smaller than about 10^{-4}–10^{-3} km^{-1} for any reasonable earth structure and vanishes for larger wave numbers. This means that Ω_3 is approximated by (56) with k_ϵ replaced by a much smaller value and hence has a main lobe that is extremely broad and of small magnitude. The first term in (58) represents a weak, large scale average of the vertically-integrated, conductivity-weighted water velocity. The second kernel $\nabla_h\Omega_4$ is similar to (57) and Figure 8, possessing the same double dipolar symmetry and a comparable spatial structure, hence the second term in (58) is also small. These observations suggest that motional magnetic fields will be very weak in an absolute sense. Motional magnetic fields have not yet been detected experimentally against the background ionospheric component except at tidal periods where the results of this paper are not valid.

The vertical magnetic field (45) also contains a dimensionless parameter kf_ψ which is nearly constant at −0.5 throughout the subinertial region of frequency-wave number space using the conductivity model of the last section. Applying the inverse Fourier transform (10) gives

$$B_- = \mu<\sigma>H\, F_-^o\Omega_5 \oplus \nabla_h\cdot<\mathbf{v}_h>^* \quad (59)$$

where Ω_5 is the inverse Fourier transform of f_ψ. With $kf_\psi \approx -0.5$, this can be approximated as

$$\Omega_5 \approx -\frac{\sqrt{2}k_\epsilon}{4\pi\rho}\left[J_0(\sqrt{2}k_\epsilon\rho) + \frac{\pi}{2}\left[J_1(\sqrt{2}k_\epsilon\rho)\mathbf{H}_0(\sqrt{2}k_\epsilon\rho) - J_0(\sqrt{2}k_\epsilon\rho)\mathbf{H}_1(\sqrt{2}k_\epsilon\rho)\right]\right] \quad (60)$$

where $\mathbf{H}_0$ and $\mathbf{H}_1$ are Struve functions. Figure 9 shows Ω_5 as given by (60). This averaging kernel is broader than that for the horizontal electric field, but not as wide as for the horizontal magnetic field. It does not have the dipolar behavior of $\nabla_h\Omega_2$ or $\nabla_h\Omega_4$. However, the motional vertical magnetic field is expected to be weak because of the small size of $\nabla_h \cdot \langle \mathbf{v}_h \rangle^*$.

The vertical electric field (51) becomes

$$E_z = -(\mathbf{v}_h \times \mathbf{F}_h^o) \cdot \hat{z} \tag{61}$$

The vertical electric field is a measure of the local geomagnetic west water velocity. Since the geomagnetic field is almost that of an axial dipole, this is nearly the zonal component at mid-latitudes. There is no spatial averaging property associated with the vertical electric field.

DISCUSSION

A simpler operational expression for the horizontal electric field that is less daunting than (55) is

$$\mathbf{E}_h = CF_z^o \hat{z} \times \langle \mathbf{v}_h \rangle^* + \mathbf{N} \tag{62}$$

where $\mathbf{N}$ is a small error term containing the second part of (55) as well as geomagnetic noise and random effects. The horizontal averaging in (55) is implicit in (62). This equation is similar to one given by *Sanford* [1971] that is in standard use:

$$\mathbf{E}_h = F_z \hat{z} \times \bar{\mathbf{v}}^* + \mathbf{J}^*/\sigma \tag{63}$$

where

$$\bar{\mathbf{v}}^* = \frac{\langle \mathbf{v}_h \rangle^*}{1+\lambda} \tag{64}$$

and λ is the ratio of the conductances of the seabed and the ocean. $\mathbf{J}^*$ represents the effect of nonlocal electric currents of which the second term in (55) is dominant in the absence of topography and ocean boundaries. By comparing (62) and (64), C is identified with $1/(1+\lambda)$. Thus, the conclusions of this paper are in agreement with those of *Sanford* [1971], although a more general treatment of seafloor conductivity is included and supported by recent geophysical data, and the spatial averaging properties of the electric field are made more explicit. However, Sanford has treated the noise terms more completely and included the effects of small topography by perturbation analysis. Because large-scale topography in the real ocean is not small compared to the average water depth, such an approach has not been applied in this paper.

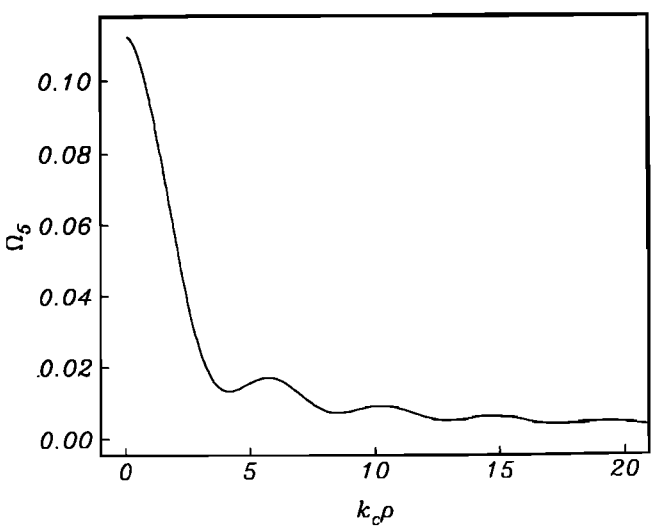

Fig. 9. Approximate form of the vertical magnetic field averaging kernel given by (60) in the text. The abscissa shows horizontal distance in units of k_c^{-1} which is of order units of water depths.

The interpretation of C in (62) as a constant of proportionality reaffirms previous results and is consistent with standard practice. While C is a function principally of the local conductivity structure, some insight into subseafloor geology is useful for assessing the effect of lateral variability of the seafloor conductivity structure on it. In the deep ocean away from major tectonic features and where sediment thickness is relatively uniform, C is likely to be invariant over a wide region. The results of Figures 4–6 suggest that C is only weakly dependent on details of the conductivity profile for a geologically reasonable set of deep ocean structures. This is supported by the observations summarized in Figure 11 of *Sanford et al.* [1985] which give $C \approx 0.91$-0.94 in the well-sedimented western North Atlantic. However, a degree of caution is needed when using (62) to compare multiple sites without individual calibrations or with submarine cable data which yield a unidirectional horizontal average of $C\langle \mathbf{v}_h \rangle^*$. In addition, different scale factors with wider variability are expected in the vicinity of mid-ocean ridges or continental margins where the reference model of *Chave et al.* [1990] may not be valid. *Larsen and Sanford* [1985] computed $C \approx 0.5$ for a cable spanning the Florida Current, suggesting a rather conductive seafloor, presumably due to the presence of 4 km thick sediments. At such locations, the effect of lateral changes in the subseafloor structure must be investigated by careful experimental calibration of the electric field over space; *Spain and Sanford* [1987] used expendable current profiler (XCP) and Pegasus data across the Florida Current for this purpose, verifying the spatial homogeneity of the seafloor conductance. It should also be noted that new terms in (62) due to ocean boundaries could appear, although the successful interpretation of the Florida Current cable data using (63) suggests that these must be small. All existing studies indicate that calibration of electric field sensors in terms of velocity is a far less serious problem than oceanographic lore holds and that boundary effects do not pose a serious limitation. In fact, the Atlantic data and geophysical model of Figure 3 indicate that simply assuming $C \approx 0.95$ would produce only small errors in the inferred integrated velocity over large tracts of the deep ocean. It should also be noted that once calibration is achieved in a given area, the scale factor C is known forever.

The seawater conductivity weighting property in (41) that appears throughout the expressions for subinertial motional electromagnetic fields serves as a filter applied to the vertical mode structure of the water velocity field. It is instructive to examine the behavior of the weighting using realistic conductivity profiles. This is accomplished by reconstructing conductivity information from zonally averaged temperature and salinity data archived by *Levitus* [1982] at a variety of latitudes and expanding the conductivity in horizontal velocity structure functions computed numerically from zonally averaged Brunt-Väisälä frequency data also taken from Levitus. From (41), it is clear that the terms in this expansion act as weights on the horizontal velocity modes. Figure 10 shows typical conductivity structures at 12.5°N and 42.5°N in the Pacific and 32.5°N and 57.5°S in the Atlantic. Table 1 shows the first five terms (barotropic plus first four baroclinic modes) in the struc-

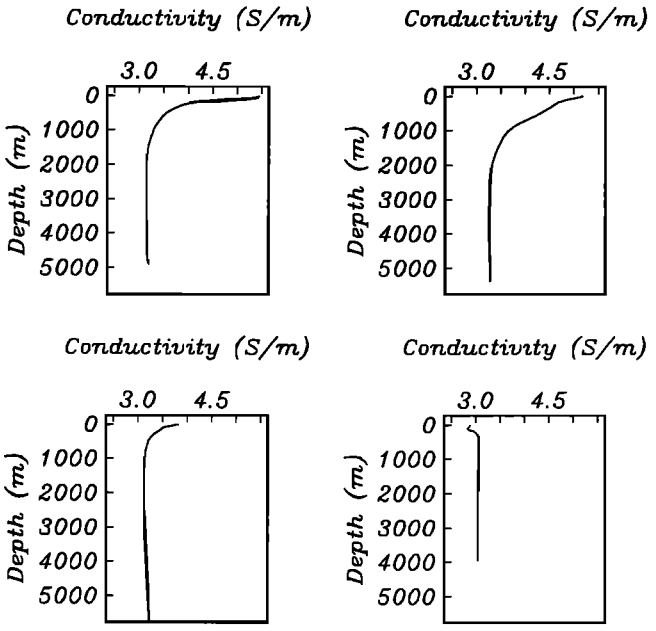

Fig. 10. Conductivity profiles computed using the empirical formulae of *Fofonoff and Millard* [1983] with zonally averaged salinity and potential temperature (converted to in situ temperature) data from *Levitus* [1982]. The locations shown are 12.5°N Pacific (upper left), 32.5°N Atlantic (upper right), 42.5°N Pacific (lower left), and 57.5°S Atlantic (lower right). The expansions of these profiles in horizontal velocity structure functions are listed in Table 1.

ture function expansion for these four profiles. In general, the barotropic mode is more accentuated and the baroclinic modes are increasingly downweighted with increasing latitude, reflecting the dominance of seawater conductivity by temperature and a concomitant shallowing of the thermocline toward the poles. To quantify this, assume that the velocity modes have identical variances. Proceeding from the equator to the pole with the entries in Table 1, this gives a horizontal electric field variance which is respectively 98.9%, 98.6%, 99.9%, and 99.99% due to the barotropic mode. Furthermore, independent information on the vertical structure of the velocity field from mooring work is available at 32.5° N in the Atlantic (the Local Dynamics Experiment during POLYMODE) and 42.5°N in the Pacific (BEMPEX). For the former, *Owens* [1985] and *Hua et al.* [1986] estimate the ratio of barotropic to baroclinic variance at 2:1 to 3:1; this translates into a 7% to 9% first baroclinic effect on the integrated current amplitude as measured by the electric field for the worst case where the direction of the modes is coincident and orthogonal to the electric measurement. Consideration of higher-order modes indicates a less than 0.5% effect for the second and third baroclinic terms and negligible effects beyond this. For BEMPEX, Luther et al. (1990) give a barotropic to baroclinic variance of about 1:2, so the effect of baroclinicity on the electric field is about 2%. These examples strongly suggest that a horizontal electrometer serves as an efficient barotropic current meter even in flows that are partially baroclinic; in the worst case examples at low latitudes, the electric field does at least as well at measuring the barotropic current as a modal separation or other depth-averaging scheme with multiple-element mooring can achieve. However, it should not be assumed that an electric field measurement is useless in the presence of strong baroclinicity where the filtering effect from conductivity weighting is less efficient at removing higher-order modes. The motion of sea level, for instance, is imperfectly dominated by the lowest vertical modes, yet this has not prohibited sea level observations from being used to study both external and internal mode phenomena. As long as the conductivity structure is known, the electric field constitutes a direct integral measurement of the ocean's velocity field with specified weighting which can serve as a strong constraint on ocean models. For a further discussion of these points and some consideration of the influence of time dependence in the conductivity structure, see Luther et al. (1990)

TABLE 1. Modal Expansion of Conductivity Profiles

Mode	12.5°N Pacific	32.5°N Atlantic	42.5°N Pacific	57.5°S Atlantic
1	3.302	3.522	3.181	3.036
2	−0.334	0.419	0.053	−0.012
3	0.116	−0.051	0.067	−0.029
4	0.002	−0.043	−0.007	−0.013
5	0.029	0.029	0.025	−0.003

This paper has primarily treated the interpretation of an electric field measured by a fixed sensor, a Eulerian situation analogous to a conventional mooring. In a moving reference frame where an instrument is dropped or towed, the electric field is a measure of the difference between the sensor velocity (vector sum of the water and platform velocities) and $C\langle \mathbf{v}_h \rangle^*$. This situation has been thoroughly treated by *Sanford* [1971] and constitutes the basis for a free-fall profiler [*Sanford et al.*, 1985] and the XCP, among others. Extension of the results of this paper to the moving sensor is straightforward and will not be considered further.

It has already been noted that motional magnetic fields have not been detected outside of the tidal band in the deep ocean. For example, *Chave et al.* [1989] showed that the seafloor magnetic field was highly coherent ($\gamma^2 \geq 0.99$) across a 300 km by 300 km array from a period of a few minutes to about 10 days (the longest period that could be studied in a statistical sense) during EMSLAB, implying that the magnetic field was dominated by external sources, while the seafloor electric field was incoherent except for a few narrow band features at periods longer than a few days. Similar seafloor magnetic field coherences across distances to 1000 km and out to periods of several months have been observed in the BEMPEX data. The reasons that motional magnetic fields are weak relative to the external part are twofold. First, the discussion around equation (58) indicates that motional magnetic fields are large-scale averages of the velocity field with a net contribution that is correspondingly small and are further reduced by the weakness of electromagnetic interactions with the earth. Second, power spectra of the horizontal magnetic field are similar at seafloor and terrestrial sites and display roughly f^{-1} behavior at periods longer than a day at mid-latitudes. The increasing external field with increasing period effectively masks any weak motional component. Even if they proved detectable, it is not clear that motional magnetic fields have real oceanographic applications because of the large scale nature of the velocity field averaging and the ambiguity of the relative sizes of the terms in (58). However, the electric field appears to be dominated by local motional sources at periods longer than a few days. This is due in part to the fact that the externally induced electric field actually decreases with increasing period below

about a day; see *Chave et al.* [1989] and Luther et al. (1990) for elaboration.

APPENDIX A: DERIVATION OF THE MODAL EQUATIONS

Using the Helmholtz representation theorem given by *Backus* [1986], any vector field on the plane may be written in terms of its vertical component, a consoidal vector field, and a toroidal vector field

$$\mathbf{T} = r\,\hat{z} + \nabla_h s + \hat{z}\times\nabla_h t \tag{A1}$$

where s and t are scalar functions which are unique up to arbitrary additive constants. Uniqueness considerations usually require that the constants be known; *Backus* [1986] suggests requiring the average value of s and t to vanish on a ball of specified radius when working with a spherical geometry. In this paper, a plane geometry will be used exclusively, and all functions will be assumed to have a spatial Fourier transform representation, so that uniqueness conditions are automatically satisfied. Combining (A1) and (1), the magnetic induction may be written in terms of scalar functions as in (5). Using (A1), the electric field is written as

$$\mathbf{E} = \alpha\,\hat{z} + \nabla_h\beta + \hat{z}\times\nabla_h\gamma \tag{A2}$$

The source current $\sigma(\mathbf{v}\times\mathbf{F})$ may be expressed in a similar way using (6). The scalar Ξ is just the vertical component of $\sigma(\mathbf{v}\times\mathbf{F})$, while the consoidal and toroidal parts of the source current in (6) are solutions of

$$\nabla_h^2\mathrm{T} = \nabla_h\cdot[\sigma(\mathbf{v}\times\mathbf{F})] \tag{A3}$$

and

$$\nabla_h^2\mathrm{Y} = (\hat{z}\times\nabla_h)\cdot[\sigma(\mathbf{v}\times\mathbf{F})]\cdot\hat{z} \tag{A4}$$

Further simplification of (A3) and (A4) for realistic ocean flows and models of the geomagnetic field are discussed in Appendix D.

Substituting (5) and (A2) into (2) gives three equations when expressed in Cartesian component form. The two horizontal components are identifiable as the Cauchy-Riemann conditions so that

$$\partial_z u_1 + i v_1 = f_1(x+iy) \tag{A5}$$

where

$$u_1 = \partial_t\Psi - \gamma \tag{A6}$$

$$v_1 = \partial_z\beta + \partial_t\Pi - \alpha \tag{A7}$$

and f_1 is an analytic function of the complex variable $x+iy$. The vertical component is the redundant statement that (A6) is harmonic. Any transformation may be made to Π and Ψ that does not alter the electromagnetic fields or violate the Maxwell equations. This makes it possible to choose $u_1=0$, as may be seen by writing out (5) for the fields under the transformation $\Psi'=\Psi-h$ where $\partial_t h=u_1$. This means that $\partial_z u_1=0$, so that f_1 is an imaginary analytic function and hence must be a constant by the Cauchy-Riemann conditions. Since a constant may be added to Π without changing (5), f_1 may be taken as zero, and two conditions on the modal scalars obtain by taking (A6) and (A7) to vanish.

It will be assumed that the electrical conductivity σ is a function only of the vertical coordinate, and that the magnetic permeability μ has the free space value everywhere. Using (3) with (5) and (6) gives the Cauchy-Riemann conditions for the horizontal components and an independent relation for the vertical one. This results in the equation

$$u_2 + i v_2 = f_2(x+iy) \tag{A8}$$

where

$$u_2 = \partial_z\Pi + \mu\sigma\beta + \mu\mathrm{T} \tag{A9}$$

and

$$v_2 = \mu\sigma\gamma + \mu\mathrm{Y} - \nabla^2\Psi \tag{A10}$$

with f_2 an analytic function, and

$$\nabla_h^2\Pi - \mu\sigma\alpha - \mu\Xi = 0 \tag{A11}$$

Since $\partial_z\Pi$ is arbitrary (this is just the choice of gauge from (5)), it is permissible to set u_2 in (A8) to zero. This requires that v_2 in (A10) be constant, but (6) is unchanged if that constant is absorbed into Y, and v_2 may also be set to zero.

Combining these conditions gives differential equations for the two modal scalar functions (7) and (8) and the electric field (9). The usual boundary conditions on the horizontal components of **E** and **B** and the vertical components of **B** and **J** must be satisfied at horizontal interfaces. These require continuity of Ψ, $\partial_z\Psi$, Π, and $(\partial_z\Pi+\mu\mathrm{T})/\mu\sigma$. Since the boundary conditions are not coupled, the PM and TM modes represented by solutions of (7) and (8) are independent.

APPENDIX B: GREEN FUNCTIONS FOR A CONSTANT CONDUCTIVITY OCEAN

Let the Cartesian coordinate system be the usual oceanographic one with $\hat{x}$ east, $\hat{y}$ north, and $\hat{z}$ positive upwards, so that the water column covers $-H\le z\le 0$, and let the conductivity of seawater be fixed at $\sigma(-H)$. Since all interfaces are assumed planar and level, the horizontal coordinates will be expressed using the Fourier transform (10), and $e^{-i\omega t}$ time dependence is assumed. Considering (13), (14), and the boundary conditions at the seafloor and sea surface, the Green functions for the PM and TM modes satisfy

$$\partial_z^2 g_\psi - \beta^2 g_\psi = \delta(z-z') \tag{B1}$$

with

$$g_\psi + \frac{1}{k}\partial_z g_\psi = 0 \quad (z=0)$$

$$g_\psi - \Lambda\partial_z g_\psi = 0 \quad (z=-H) \tag{B2}$$

and

$$\partial_z^2 g_\pi - \beta^2 g_\pi = \delta(z-z') \tag{B3}$$

with

$$g_\pi = 0 \quad (z=0)$$

$$g_\pi - \mathrm{K}/\sigma(-H)\partial_z g_\pi = \mu\mathrm{K}\tilde{\mathrm{T}}/\sigma(-H) \quad (z=-H) \tag{B4}$$

where β is given by (16). The functions Λ and K specify the structure beneath the seafloor and are the ratios of the boundary conditions at the interfaces. They will appear in the Green functions through complex reflection coefficients whose computation for a layered earth structure is discussed in Appendix C.

Obtaining the PM mode solution for (B1) and (B2) is straightforward using the method of variation of parameters. The complete Green function is given by

$$g_\psi(z,z') = -\left[e^{-\beta|z-z'|} + R_L^{PM}e^{-\beta(z+z'+2H)} + R_A^{PM}e^{\beta(z+z')} + R_A^{PM}R_L^{PM}e^{\beta(|z-z'|-2H)}\right] / \left[2\beta(1-R_A^{PM}R_L^{PM}e^{-2\beta H})\right] \quad \text{(B5)}$$

where the solution to (7) is

$$\tilde{\Psi} = \mu\int_{-H}^{0} dz'\, g_\psi(z,z')\tilde{Y}(z') \quad \text{(B6)}$$

The reflection coefficients at the sea surface and seafloor are given by

$$R_A^{PM} = (\beta-k)/(\beta+k) \quad \text{(B7)}$$

and

$$R_L^{PM} = (\beta\Lambda-1)/(\beta\Lambda+1) \quad \text{(B8)}$$

Note that this definition is opposite in sign to the conventional optics one.

The TM mode Green function g_π for homogeneous boundary conditions follows immediately from (B5) by replacing the sea surface reflection coefficient with -1 and the seafloor one with R_L^{TM}, giving

$$g_\pi(z,z') = -\left[e^{-\beta|z-z'|} + R_L^{TM}e^{-\beta(z+z'+2H)} - e^{\beta(z+z')} - R_L^{TM}e^{\beta(|z-z'|-2H)}\right] / \left[2\beta(1+R_L^{TM}e^{-2\beta H})\right] \quad \text{(B9)}$$

where the TM mode seafloor reflection coefficient is given by

$$R_L^{TM} = (\beta K/\sigma(-H)-1)/(\beta K/\sigma(-H)+1) \quad \text{(B10)}$$

A solution for Π analogous to (B6) is then added to a solution of the homogeneous form of (B3) which satisfies the inhomogeneous form of the boundary conditions (B4). Integrating by parts gives the full solution to (8):

$$\tilde{\Pi}(z) = \mu\int_{-H}^{0} dz'\, g_\pi(z,z')\tilde{\Xi}(z') + \mu\int_{-H}^{0} dz'\, \partial_{z'}g_\pi(z,z')\tilde{T}(z') \quad \text{(B11)}$$

The z derivative of (B5) and both the z and z' first derivatives and the mixed second derivative of (B9) are needed to get the field components. Note that all of the first derivatives are discontinuous at $z=z'$, while $\partial_z\partial_{z'}g_\pi$ possesses a delta function discontinuity at the same point, as seen in (34).

APPENDIX C: REFLECTION COEFFICIENTS

Consider a stack of L layers below the seafloor each having thickness h_l and electrical conductivity σ_l. Let $z=-z_l$ denote the base of each layer and terminate the stack in a half-space of conductivity σ_{L+1} beginning at $z=-z_L$.

The PM mode response function Λ introduced in Appendix B is

$$\Lambda = \frac{\tilde{\Psi}(-H)}{\partial_z\tilde{\Psi}(-H)} \quad \text{(C1)}$$

This may be generalized so that Λ_l denotes the ratio at the ith interface and $\Lambda_0\equiv\Lambda$ is the surface value (C1) used in (B8). In a similar way, the reflection coefficient may be generalized so that R_l^{PM} denotes the value at the ith internal interface and R_0^{PM} is the surface value. The PM mode scalar $\tilde{\Psi}$ satisfies the homogeneous form of (13) with $\sigma(z)=\sigma_l$ in the ith layer. Using the solution of this with the continuity conditions at the interfaces, it is simple to derive a recursive expression for Λ_l in terms of Λ_{l+1}:

$$\Lambda_l = \frac{\beta_{l+1}\Lambda_{l+1} + \tanh(\beta_{l+1}h_{l+1})}{\beta_{l+1}[1+\beta_{l+1}\tanh(\beta_{l+1}h_{l+1})\Lambda_{l+1}]} \quad \text{(C2)}$$

where

$$\beta_l = \sqrt{k^2 - i\omega\mu\sigma_l} \quad \text{(C3)}$$

The ith reflection coefficient and the ith response function are related by

$$\Lambda_l = \frac{1+R_l^{PM}}{\beta_l(1-R_l^{PM})} \quad \text{(C4)}$$

Combining (C2) and (C4) gives an expression for the ith reflection coefficient in terms of the (i+1)th one:

$$R_l^{PM} = \frac{\alpha_l + e^{-2\beta_{l+1}h_{l+1}}R_{l+1}^{PM}}{1+\alpha_l e^{-2\beta_{l+1}h_{l+1}}R_{l+1}^{PM}} \quad \text{(C5)}$$

where the interface reflection coefficient is

$$\alpha_l = \frac{\beta_l - \beta_{l+1}}{\beta_l + \beta_{l+1}} \quad \text{(C6)}$$

This is initialized at $z=-z_L$ with α_L for a conducting half-space or -1 when the half-space is replaced by a perfect conductor.

The TM mode response function is defined by

$$K = \frac{\sigma(-H)\tilde{\Pi}(-H)}{\partial_z\tilde{\Pi}(-H)} \quad \text{(C7)}$$

and may be generalized to the ith interface in the same manner as the PM mode one. Following the same procedure, the recursion relation is

$$R_l^{TM} = \frac{\chi_l + e^{-2\beta_{l+1}h_{l+1}}R_{l+1}^{TM}}{1+\chi_l e^{-2\beta_{l+1}h_{l+1}}R_{l+1}^{TM}} \quad \text{(C8)}$$

where the interface reflection coefficient is

$$\chi_l = \frac{\beta_l\sigma_{l+1} - \beta_{l+1}\sigma_l}{\beta_l\sigma_{l+1} + \beta_{l+1}\sigma_l} \quad \text{(C9)}$$

The recursion relation is initialized at $z=-z_L$ with χ_L for a conducting half-space, 1 if the half-space is a replaced by a perfect conductor, or -1 if the half-space is replaced by an insulator.

Use of the recursive forms (C5) and (C8) results in superior numerical behavior when compared to recursions for the response functions (C1) and (C7) as given by *Chave and Cox* [1982].

APPENDIX D: SOURCE CURRENT TERMS FOR AN INCLINED GEOCENTRIC GEOMAGNETIC FIELD

In the standard oceanographic coordinate system an inclined geocentric dipole model for the geomagnetic field yields

$$F_x = (\frac{a}{\zeta})^3[g_1^1\sin\phi - h_1^1\cos\phi]$$

$$F_y = -(\frac{a}{\zeta})^3[g_1^0\cos\lambda - (g_1^1\cos\phi + h_1^1\sin\phi)\sin\lambda]$$

$$F_z = 2(\frac{a}{\zeta})^3[g_1^0\sin\lambda + (g_1^1\cos\phi + h_1^1\sin\phi)\cos\lambda] \quad \text{(D1)}$$

where $a \approx 6371$ km is the mean radius of the earth, ζ is the observation radius relative to the center of the earth, λ is the latitude, ϕ is the longitude relative to Greenwich, and $\{g_l^j, h_l^j\}$ are the Gauss coefficients for the geomagnetic field given most recently by *IAGA Division I Working Group 1* [1988]. Since the depth of the ocean is much smaller than the radius of the earth, a/ζ in (D1) may be replaced with 1 except when vertical derivatives are taken.

In a similar spirit to that of the beta-plane approximation, a reference latitude λ_o and longitude ϕ_o are chosen and approximate derivatives of the geomagnetic field are computed on a tangent plane using a first-order Taylor expansion with $\lambda \approx \lambda_o + y/a$, $\phi \approx \phi_o + x/a$, where x,y are assumed small compared to a. The expression (D1) becomes

$$\mathbf{F} = \mathbf{F}^o + \overleftrightarrow{\alpha}\cdot\mathbf{r} \tag{D2}$$

where the components of $\mathbf{F}^o$ are given by (D1) at (λ_o, ϕ_o) with $a/\zeta = 1$ and $\mathbf{r} = x\hat{x} + y\hat{y} + z\hat{z} = \vec{\rho} + \hat{z}$ is the radius vector relative to the center of the tangent plane at the sea surface. The geomagnetic gradient tensor $\overleftrightarrow{\alpha}$ is given by

$$\overleftrightarrow{\alpha} = \begin{bmatrix} \alpha_x^x & \alpha_y^x & \alpha_z^x \\ \alpha_x^y & \alpha_y^y & \alpha_z^y \\ \alpha_x^z & \alpha_y^z & \alpha_z^z \end{bmatrix} \tag{D3}$$

with elements

$$\alpha_x^x = [g_1^1 \cos\phi_o + h_1^1 \sin\phi_o]/a$$

$$\alpha_x^y = 0$$

$$\alpha_x^z = -3\,[g_1^1 \sin\phi_o - h_1^1 \cos\phi_o]/a$$

$$\alpha_y^x = -[g_1^1 \sin\phi_o - h_1^1 \cos\phi_o]\sin\lambda_o/a$$

$$\alpha_y^y = [g_1^0 \sin\lambda_o + (g_1^1 \cos\phi_o + h_1^1 \sin\phi_o)\cos\lambda_o]/a$$

$$\alpha_y^z = 3\,[g_1^0 \sin\lambda_o + (g_1^1 \cos\phi_o + h_1^1 \sin\phi_o)\cos\lambda_o]/a$$

$$\alpha_z^x = -2\,[g_1^1 \sin\phi_o - h_1^1 \cos\phi_o]\cos\lambda_o/a$$

$$\alpha_z^y = 2\,[g_1^0 \cos\lambda_o - (g_1^1 \cos\phi_o + h_1^1 \sin\phi_o)\sin\lambda_o]/a$$

$$\alpha_z^z = -6\,[g_1^0 \sin\lambda_o + (g_1^1 \cos\phi_o + h_1^1 \sin\phi_o)\cos\lambda_o]/a$$

Separating the horizontal and vertical components of water velocity and using some standard vector identities, the source current equations (A5) and (A6) may be written

$$\nabla_h^2 \mathrm{T} = \sigma \left[(F_z^o \nabla_h + \nabla_h F_z^o) \times \mathbf{v}_h \cdot \hat{z} - (\hat{z} \times \nabla_h \mathrm{v}_z) \cdot \mathbf{F}_h \right] \tag{D4}$$

$$\nabla_h^2 \mathrm{Y} = -\sigma \left[(\nabla_h \cdot \mathbf{v}_h + \mathbf{v}_h \cdot \nabla_h) F_z^o + (\mathbf{F}_h^o \cdot \nabla_h + \nabla_h \cdot \mathbf{F}_h) \mathrm{v}_z \right] \tag{D5}$$

With (D2) and (D3), (D4) and (D5) together with the vertical source current can be reduced to

$$\Xi = \sigma[\mathbf{v}_h \times \mathbf{F}_h^o + \mathbf{v}_h \times (\overleftrightarrow{\alpha}\cdot\mathbf{r})_h] \cdot \hat{z} \tag{D6}$$

$$\nabla_h^2 \mathrm{T} = \sigma \left[\left[(F_z^o + \overleftrightarrow{\alpha}\cdot\mathbf{r}\cdot\hat{z}) \nabla_h + \nabla_h (\overleftrightarrow{\alpha}\cdot\mathbf{r}\cdot\hat{z}) \right] \times \mathbf{v}_h \cdot \hat{z} - \left[\mathbf{F}_h^o + (\overleftrightarrow{\alpha}\cdot\mathbf{r})_h \right] \cdot (\hat{z} \times \nabla_h \mathrm{v}_z) \right] \tag{D7}$$

$$\nabla_h^2 \mathrm{Y} = -\sigma \left[\left[F_z^o + \overleftrightarrow{\alpha}\cdot\mathbf{r}\cdot\hat{z} \right] \nabla_h \cdot \mathbf{v}_h + (\overleftrightarrow{\alpha}\cdot\mathbf{v}_h \cdot \hat{z}) \cdot \left[(\mathbf{F}_h^o + \overleftrightarrow{\alpha}\cdot\mathbf{r}) \cdot \nabla_h + \nabla_h \cdot \overleftrightarrow{\alpha}\cdot\mathbf{r} \right] \mathrm{v}_z \right] \tag{D8}$$

where $\overleftrightarrow{\alpha}\cdot\mathbf{r}\cdot\hat{z} \approx \overleftrightarrow{\alpha}\cdot\vec{\rho}\cdot\hat{z}$.

For the frequency range of interest in the real ocean the vertical velocity is small compared to the horizontal one, and the terms in the vertical velocity in (D7) and (D8) may be neglected. The terms in the field gradients are neglected in the treatment in the text, although it is relatively simple to incorporate them. Their effect can be included by replacing the magnetic field terms in the text with (D2). However, it should be remembered that the approximations used in this appendix are formally valid only for horizontal length scales small compared to the radius of the earth, and that a more complete analysis on a sphere is needed at larger scales.

NOTATION

$\mathbf{B}$	magnetic induction, Wb/m^2
$\mathbf{E}$	electric field, V/m^2
f_ψ	approximate PM mode Green function (29)
g_π	TM mode Green function (B9)
g_ψ	PM mode Green function (B5)
h_ψ	approximate PM mode Green function vertical derivative (30)
h_π	approximate TM mode Green function kernel (35)
$\mathbf{F}$	magnetic induction of the earth, Wb/m^2 (D2)
F_z^o	vertical component of geomagnetic induction at latitude λ_o and longitude ϕ_o (D1)
H	water depth, m
$\mathbf{I}$	induced electric current density $\sigma\mathbf{E} = \mathbf{J} - \sigma\mathbf{v}\times\mathbf{F}$, A/m^2
$\mathbf{J}$	total electric current density, A/m^2 (4)
$\mathbf{k}$	horizontal wave number (η,ξ), rad/m
R_A^{PM}	dimensionless PM mode atmospheric reflection coefficient (B7)
R_L^{PM}	dimensionless PM mode seafloor reflection coefficient (B8), (C5)
R_L^{TM}	dimensionless TM mode seafloor reflection coefficient (B10), (C8)
T_L^{TM}	dimensionless TM mode seafloor transmission coefficient (28)
$\mathbf{v}_h$	horizontal water velocity, m/s
β	self induction parameter (16)
ε	dimensionless induction number (23)
θ	azimuthal angle with respect to the x axis, rad
λ	geographic latitude, rad
μ	magnetic permeability of free space $4\pi\times10^{-7}$ h/m
ν	electrical permittivity, f/m
Ξ	vertical component of source current density, A/m^2 (6)
Π	TM mode scalar, Wb/m (5)
ρ	horizontal distance $(x^2+y^2)^{1/2}$, m
σ	electrical conductivity, S/m
T	scalar for horizontally divergent (consoidal) part of source current density, A/m (6), (A3)
Y	scalar for nondivergent (toroidal) part of source current density, A/m (6), (A4)
ϕ	geographic longitude relative to Greenwich, rad
Ψ	PM mode scalar, Wb (5)
ω	angular frequency, rad/s
∇_h	horizontal gradient operator $\partial_x\hat{x} + \partial_y\hat{y}$
$\Delta\sigma$	difference between the in situ seawater

conductivity and the seafloor value, S/m (15)
$\langle\sigma\rangle$ depth-averaged seawater conductivity, S/m (40)
$\langle \mathbf{v}_h \rangle^*$ vertically-integrated, conductivity-weighted water velocity, m/s (41)
$\hat{k}$ unit vector in the propagation direction
$\hat{x},\hat{y},\hat{z}$ unit vectors in the east, north, and up directions, respectively

Acknowledgments. It is a pleasure to acknowledge numerous fruitful discussions about motional electromagnetic induction with C.S. Cox and T.B. Sanford. This research has been supported at SIO by NSF grants OCE84-20578 and OCE88-00783.

REFERENCES

Backus, G.E., The electric field produced in the mantle by the dynamo in the core, *Phys. Earth. Planet. Inter.*, *28*, 191–214, 1982.

Backus, G.E., Poloidal and toroidal fields in geomagnetic field modeling, *Rev. Geophys*, *24*, 75–109, 1986.

Chave, A.D., and C.S. Cox, Controlled electromagnetic sources for measuring electrical conductivity beneath the oceans, 1, Forward problem and model study, *J. Geophys. Res.*, *87*, 5327–5338, 1982.

Chave, A.D., J.H. Filloux, D.S. Luther, L.K. Law, and A. White, Observations of motional electromagnetic fields during EMSLAB, *J. Geophys. Res.*, *94*, 14153–14166, 1989.

Chave, A.D., A. Flosadóttir, and C.S. Cox, Some comments on seabed propagation of ULF/ELF electromagnetic fields, *Radio Sci.*, in press, 1990.

Cox, C.S., On the electrical conductivity of the oceanic lithosphere, *Phys Earth. Planet. Inter*, *25*, 196–201, 1981.

Cox, C.S., S.C. Constable, A.D. Chave, and S.C. Webb, Controlled source electromagnetic sounding of the oceanic lithosphere, *Nature*, *320*, 52–54, 1986.

Faraday, M., Experimental researches in electricity (Bakerian Lecture), *Philos. Trans. R. Soc. London*, *122*, 163–177, 1832.

Fofonoff, N.P., and R.C. Millard, Algorithms for computation of fundamental properties of seawater, *UNESCO Tech. Pap. Mar. Sci.*, *44*, 53 pp., 1983.

Harvey, R.R., Derivation of oceanic water motions from measurement of the vertical electric field, *J. Geophys. Res.*, *79*, 4512–4516, 1974.

Hohmann, G.W., Three-dimensional EM modeling, *Geophys. Surv.*, *6*, 27–53, 1983.

Hua, B.L., J.C. McWilliams, and W.B. Owens, An objective analysis of the POLYMODE Local Dynamics Experiment, II, Streamfunction and potential vorticity fields during the intensive period, *J Phys Oceanogr.*, *16*, 506–522, 1986.

IAGA Division I Working Group 1, International Geomagnetic Reference Field revision 1987, *Geophys J*, *93*, 187–189, 1988.

Larsen, J.C., and T.B. Sanford, Florida Current volume transport from voltage measurements, *Science*, *227*, 302–304, 1985.

Levitus, S., Climatological atlas of the world ocean, *NOAA Prof. Pap.*, *13*, 173pp., U.S. Govt. Print. Off., Washington D.C., 1982.

Longuet-Higgins, M.S., The electrical and magnetic effects of tidal streams, *Mon. Not. R. astron. Soc., Geophys. Suppl.*, *5*, 285–307, 1949.

Longuet-Higgins, M.S., M.E. Stern, and H. Stommel, The electric field induced by ocean currents and waves, with applications to the method of towed electrodes, *Papers Phys. Oceanogr. Meteorol.*, *13*, 1–37, 1954.

Luther, D.S., Evidence of a 4–6 day barotropic, planetary oscillation of the Pacific Ocean, *J Phys. Oceanogr.*, *12*, 644–657, 1982.

Luther, D.S., A.D. Chave, and J.H. Filloux, BEMPEX: A study of barotropic ocean currents and lithospheric electrical conductivity, *EOS Trans. AGU*, *68*, 618–619, 628–629, 1987.

Malkus, W.V.R., and M.E. Stern, Determination of ocean transports and velocities by electromagnetic effects, *J Mar Res*, *11*, 97–103, 1952.

Owens, W.B., A statistical description of the vertical and horizontal structure of eddy variability on the edge of the Gulf Stream recirculation, *J. Phys. Oceanogr*, *15*, 195–205, 1985.

Sanford, T.B., Motionally-induced electric and magnetic fields in the sea, *J. Geophys. Res.*, *76*, 3476–3492, 1971.

Sanford, T.B., Temperature transport and motional induction in the Florida Current, *J. Mar Res.*, *40, Suppl*, 621–639, 1982.

Sanford, T.B., Recent improvements in ocean current measurement from motional electric fields and currents, *Proc. IEEE Third Working Conf. Current Measurement*, 65–76, 1986.

Sanford, T.B., R.G. Drever, and J.H. Dunlap, An acoustic doppler and electromagnetic velocity profiler, *J. Atmos Ocean. Tech.*, *2*, 110–124, 1985.

Spain, P.F., and T.B. Sanford, Accurately monitoring the Florida Current with motionally induced voltages, *J. Mar. Res.*, *45*, 843–870, 1987.

Stommel, H., The theory of the electric field induced by deep ocean currents, *J. Mar. Res.*, *8*, 386–392, 1948.

von Arx, W.S., An electromagnetic method for measuring the velocities of ocean currents from a ship under way, *Papers Phys. Oceanogr. Meteorol*, *11*, 1–62, 1950.

Wertheim, G.K., Studies of the electrical potential between Key West, Florida and Havana, Cuba, *Trans. Am. Geophys. Un.*, *35*, 872–882, 1954.

A.D. Chave, AT&T Bell Laboratories, 600 Mountain Ave., Murray Hill, NJ 07974.

D.S. Luther, Scripps Institution of Oceanography, A-030, La Jolla, CA 92093.

(Received August 16, 1989;
accepted October 23, 1989.)